History of Galaxy Interactions and Their Impact on Star Formation over the Last 7 Gyr from GEMS

Shardha Jogee [1], Sarah H. Miller [1], Kyle Penner [1], Rosalind E. Skelton [2], Christopher J. Conselice [3], Rachel S. Somerville [2], Eric F.Bell [2], Xian Zhong Zheng [4], Hans-Walter Rix [2], Aday R. Robaina [2], Fabio D. Barazza [5], Marco Barden [6], Andrea Borch [2], Steven V.W. Beckwith [7], John A. R.Caldwell [8], Chien Y. Peng [9], Catherine Heymans [10], Daniel H. McIntosh [11], Boris Häußler [2], Knud Jahnke [2], Klaus Meisenheimer [2], Sebastian F. Sanchez [12], Lutz Wisotzki [13], Christian Wolf [14] Casey Papovich [15],

sj@astro.as.utexas.edu

[1]Department of Astronomy, University of Texas at Austin, 1 University Station C1400, Austin, TX 78712-0259

[2]Max-Planck-Institut für Astronomie, Königstuhl 17, D-69117,Heidelberg, Germany

[3]School of Physics and Astronomy, The University of Nottingham, University Park, Nottingham NG7 2RD, UK

[4]Purple Mountain Observatory, Nanjing, China.

[5]Laboratoire d'Astrophysique, École Polytechnique Fédérale de Lausanne (EPFL), Observatoire, 1290 Sauverny, Switzerland

[6]Institute for Astro- and Particle Physics, University of Innsbruck, Technikerstr. 25/8, A-6020 Innsbruck, Austria

[7]Department of Physics and Astronomy, Johns Hopkins University, Charles and 4th Street, Baltimore, MD 21218

[8]University of Texas, McDonald Observatory, Fort Davis TX, 79734 USA

[9]NRC Herzberg Institute of Astrophysics, Victoria, Canada

[10]SUPA,Institute for Astronomy, University of Edinburgh, Royal Observatory, Edinburgh EH9 3HJ

[11]Department of Astronomy, University of Massachusetts, 710 North Pleasant Street, Amherst, MA 01003, USA

[12]Centro Astronmico Hispano Alemn, Calar Alto, CSIC-MPG, C/Jess Durbn Remn 2-2, E-04004 Almeria, Spain

[13]Astrophysikalisches Institut Potsdam, An der Sternwarte 16, D-14482 Potsdam, Germany

[14]Astrophysics, University of Oxford, Keble Road, Oxford OX1 3RH, U.K.

[15]Department of Astronomy, University of Arizona, Steward Observatory, 933 N. Cherry Avenue, Tucson,

ABSTRACT

We perform a comprehensive estimate of the frequency of interacting galaxies and their impact on the SFR over $z \sim 0.24$–0.80 (lookback time $T_b \sim 3$–7 Gyr), using ~ 3600 ($M \geq 1 \times 10^9\ M_\odot$) galaxies with GEMS HST, COMBO-17, and Spitzer data. Our results are: (1) Among ~ 790 high mass ($M \geq 2.5 \times 10^{10}\ M_\odot$) galaxies, the fraction of visually-classified interacting galaxies over $z \sim 0.24$–0.80, ranges from $9\% \pm 5\%$ to $8\% \pm 2\%$. Lower limits on the major merger and minor merger fraction over this interval range from 1.1% to 3.5% , and 3.6% to 7.5%, respectively. This is the first, albeit approximate, empirical estimate of the frequency of minor mergers over the last 7 Gyr. Assuming a visibility time of ~ 0.5 Gyr, it follows that over $z \sim 0.24$–0.80, each massive galaxy undergoes ~ 0.7 mergers of mass ratio $> 1/10$, with $\sim 1/4$, $2/3$, and 10% of these being, respectively, major, minor, or ambiguous 'major or minor' mergers. The merger rate is $\sim$ a few $\times 10^{-4}$ galaxies $\mathrm{Gyr}^{-1}\ \mathrm{Mpc}^{-3}$. Among ~ 2840 blue cloud galaxies of mass $M \geq 1.0 \times 10^9\ M_\odot$, similar results hold. (2) We compare the empirical merger rate for high mass galaxies to three ΛCDM-based models: halo occupation distribution models, semi-analytic models, and hydrodynamic SPH simulations. We find qualitative agreement between observations and models, with the (major+minor) merger rate from different models bracketing the observed rate, and showing a factor of five dispersion. Near-future improvements can now start to rule out certain merger scenarios. (3) Among $\sim 3600\ M \geq 1.0 \times 10^9\ M_\odot$ galaxies, we find that the mean SFR of visibly interacting galaxies is only modestly enhanced compared to non-interacting galaxies over $z \sim 0.24$–0.80. Visibly interacting systems only account for a small fraction ($< 30\%$) of the cosmic SFR density over $T_b \sim 3$–7 Gyr, consistent with the results of Wolf et al. (2005) over $T_b \sim 6.2$–6.8 Gyr. This suggests that the behavior of the cosmic SFR density over the last 7 Gyr is predominantly shaped by non-interacting galaxies.

Subject headings: galaxies: fundamental parameters — galaxies: structure — galaxies: kinematics and dynamics — galaxies: evolution

AZ 85721

1. Introduction

Hierarchical Λ cold dark matter (ΛCDM) models provide a successful paradigm for the growth of dark matter on large scales. The evolution of galaxies within ΛCDM cosmogonies depends on the baryonic merger history, the star formation (SF) history, the nature and level of feedback from supernovae and AGN, the redistribution of angular momentum via bars or mergers, and other aspects of the baryonic physics. Empirical constraints on the fate of the baryonic component, in particular their merger and SF history, are key for developing a coherent picture of galaxy evolution and testing galaxy evolution models (e.g., Kauffmann et al. 1993; Somerville & Primack 1999; Navarro & Steinmetz 2000; Murali et al. 2002; Governato et al. 2004; Maller et al. 2006). Such constraints can help to resolve several major areas of discord between observations and ΛCDM models of galaxy evolution, such as the angular momentum crisis, the problem of bulgeless and low bulge-to-total (B/T) ratio galaxies (Navarro & Benz 1991; D'Onghia & Burkert & 2004; Kautsch et al. 2006; Barazza, Jogee, & Marinova 2007; Weinzirl et al. 2008), and the substructure problem.

The merger history of galaxies impacts the mass assembly, star formation history, AGN activity and structural evolution of galaxies. Yet, the merger rate has proved hard to robustly measure for a variety of reasons. Initially, small samples hindered the first efforts to measure merger rates (Patton et al. 2000; Le Fevre et al. 2000; Conselice et al. 2003). Later studies drew from larger samples, and have used a variety of methods to characterize the interaction history of galaxies at $z < 1$. Studies based on close pairs report a major merger fraction of $\sim$ 2% to 10% over z$\sim$ 0.2 to 1.2 (Kartaltepe et al 2007; Lin 2004) and $\sim$ 5% for massive galaxies at z$\sim$ 0.4 to 0.8 (Bell et al 2006). Studies based on Gini-M20 coefficients report a fairly constant fraction ($\sim$ 7 $\pm$ 0.2 %) of disturbed galaxies over z$\sim$ 0.2 to 1.2 among bright galaxies (Lotz et al 2008) in the AEGIS survey. Similar trends are found from early results based on visual classification and asymmetry parameters of high mass galaxies (e.g., Jogee et al. 2008). The study by Cassata et al. (2005) based on both pairs and asymmetries report a flat evolution of the merger rate with redshift up to z$\sim$ 1. The merger rate/fraction at $z > 1$ remains highly uncertain, owing to relatively modest volumes and bandpass shifting effects, but with a general trend towards higher merger fractions at higher redshifts (Conselice et al. 2003; Cassata et. al. 2005).

Studies to date have brought important insights but face several limitations. The use of automated parameters, such as CAS asymmetry A and clumpiness parameters (Conselice et al. 2000; Conselice 2003) or Gini-M20 coefficients (e.g., Lotz et al. 2004) to identify merging galaxies can fail to pick stages of major or minor mergers where distortions do not dominate the total light contribution (§ 3.4). Comparison with simulations suggest that the CAS criterion ($A > 0.35$ and $A > S$; Conselice 2003) capture major mergers about 1/3 of the

time, while the eye is sensitive to major merger features over twice as long (e.g., Conselice 2006; § 3.4). To complicate matters, automated asymmetry parameters can also capture non-interacting galaxies hosting small-scale asymmetries that are produced by stochastic star formation (§ 3.4). In the case of studies based on close (separation $\sim$ 5 to 30 kpc) pairs, the translation of the pair frequency into a merger rate is somewhat uncertain due to several factors. The uncertainties in the spectrophotometric redshifts for some of the galaxies in pairs can cause us to overestimate or underestimate the true close pair fraction, with the latter effect being more likely. Corrections for this effect are uncertain and depend on the shape of the spectrophotometric redshift errors (e.g., see Bell et al. 2006 for discussion). Secondly, even pairs with members at the same redshift may not be gravitationally bound, and may therefore not evolve into a merger in the future: this effect causes the close pair fraction to be upper limits for the merger fraction. Thirdly, gravitationally bound pairs captured by this method sample different phases of an interaction depending on the separation, and any merger rate inferred depends on the separation, orbital eccentricity, and orbital geometry.

In this paper, we present a complementary study of the frequency and impact of strong galaxy interactions on the SF activity of galaxies over $z \sim$ 0.24–0.80 (lookback times $T_{\rm b}$ of 3–7 Gyr[1]) using HST ACS, COMBO-17, and Spitzer 24 μm data of $\sim$ 3600 galaxies in the GEMS survey. The outline of the paper is given below and describes how this study complements existing work:

1. We use a large sample of $\sim$ 3600 ($M \geq 1 \times 10^9$ $M_\odot$) galaxies to get robust number statistics for the fraction of interacting galaxies among $\sim$ 790 high mass ($M \geq 2.5 \times 10^{10}$ $M_\odot$) galaxies and $\sim$ 2840 $M \geq 1 \times 10^9$ $M_\odot$ blue cloud galaxies (§ 2; Table 1; Table 2).

2. Two independent methods are used to identify strongly interacting galaxies: a tailored visual classification system complemented with spectrophotometric redshifts and stellar masses (§ 3.2), as well as automated CAS asymmetry and clumpiness parameters (§ 3.4). This allows one of the most extensive comparisons to date between CAS-based and visual classification results (§ 4.2).

3. We set up this visual classification system, to target interacting systems whose morphology and other properties suggest they are a recent merger of mass ratio $M1/M2 > 1/10$. Throughout this paper, we use the standard definition whereby major mergers are defined to have stellar mass ratio ($1/4 < M1/M2 \leq 1/1$), while minor mergers have ($1/10 < M1/M2 \leq 1/4$). By dividing the systems into 'major', 'minor', and ambiguous 'major or minor' mergers (§ 3.3), we set lower limits on the major and minor merger fraction. To our knowledge, this is the first, albeit approximate, empirical estimate of

---

[1]We assume a flat cosmology with $\Omega_{\rm m,0} =$ 1- $\Omega_\lambda =$ 0.3 and H$_0 =$ 70 km s^{-1} Mpc^{-1} throughout.

the frequency of minor mergers over the last 7 Gyr. While many earlier studies focused on major mergers, it is important to constrain minor mergers as well, since they dominate the merger rates in ΛCDM models.

4. We compare the merger rate R to a suite of ΛCDM-based simulations of galaxy evolution, including halo occupation distribution models, semi-analytic models, and hydrodynamic SPH simulations (§ 4.5). To our knowledge, such extensive comparisons have not been attempted to date, and are long overdue.

5. The idea that galaxy interactions generally enhance the SFR of galaxies is well established from observations (e.g., Larson & Tinsley 1978; Joseph & Wright 1985; Kennicutt et al. 1987; Barton et al 2003) and simulations (e.g., Negroponte & White 1983; Hernquist 1989; Barnes & Hernquist 1991, 1996; Mihos & Hernquist 1994, 1996; Springel, Di Matteo & Hernquist 2005). However, simulations cannot uniquely predict the factor by which interaction enhance the SF activity of galaxies over the last 7 Gyr, since both the SFR and properties of the remnants in simulations are highly sensitive to the stellar feedback model, the bulge-to-disk (B/D) ratio, the gas mass fractions, and orbital geometry (e.g., Cox et al 2006; di Matteo et al. 2007). Thus, in § 4.6, we investigate the impact of interactions on the average UV-based and UV+IR-based SFR of intermediate-to-high mass ($M \geq 1 \times 10^9 \ M_\odot$) galaxies over $z \sim 0.24$–0.80.

6. The SF properties of interacting and non-interacting galaxies since $z < 1$ is of great astrophysical interest, given that the cosmic SFR density is claimed to decline by a factor of 4 to 10 since $z \sim 1$ (e.g., Lilly et al. 1996; Ellis et al 1996; Flores et al. 1999; Haarsma et al. 2000; Hopkins 2004; Pérez-González et al. 2005; Le Floc'h et al. 2005). In § 4.7, we set quantitative limits on the contribution of obviously interacting systems to the UV-based and UV+IR-based SFR density over $z \sim 0.24$–0.80. Our study covers a 4 Gyr interval ($T_b \sim 3$–7 Gyr or $z \sim 0.24$–0.80) and extends the earlier studies carried out over a smaller 0.6 Gyr interval ($T_b \sim 6.2$–6.8 Gyr or $z \sim 0.65$–0.75) by Wolf et al. (2005) and Bell et al. (2005) on the UV and IR luminosity density, respectively. Our study also complements earlier IR-based studies by Hammer et al. (2005; l95 galaxies at $z > 0.4$) and Melbourne et al. (2005; ~ 800 galaxies) in terms of better number statistics and the use of both UV-based and IR-based SFR indicators.

7. Finally, our results are summarized in § 5.

2. Dataset and Sample Selection

This study uses data from the Galaxy Evolution from Morphology and SEDS (GEMS; Rix et al. 2004) survey, which provides high resolution *Hubble Space Telescope (HST)* Ad-

vanced Camera for Surveys (ACS) images in the F606W and F850LP filters over an 800 arcmin^2 ($\sim 28' \times 28'$) field centered on the Chandra Deep Field-South (CDF-S). Accurate spectrophotometric redshifts [$\delta_z/(1 + z) \sim 0.02$ down to $R_{\mathrm{Vega}} = 24$] and spectral energy distributions, based on 5 broad bands ($UBVRI$) and 12 medium band filters, are available from the COMBO-17 project (Wolf et al. 2004). The ACS data reach a limiting $5\,\sigma$ depth for point sources of 28.3 and 27.1 AB mag in F606W and F850LP, respectively (Rix et al. 2004; Caldwell et al. 2008). The effective point spread function (PSF) in a single F606W image is $\sim 0\farcs07$, corresponding to 260 pc at $z \sim 0.24$ and 520 pc at $z \sim 0.80$. In addition to HST ACS imaging, the GEMS field has panchromatic coverage which includes $Spitzer$ (Rieke et al. 2004; Papovich et al. 2004) and $Chandra$ data (Alexander et al. 2003; Lehmer et al. 2005). We use stellar masses from Borch et al. (2006) based on their SED fitting. They use the PEGASE stellar population synthesis model and a Kroupa (Kroupa et al. 1993) initial mass function (IMF) adopted in the mass regime 0.1–120 $M_{\odot}$. Such stellar masses are consistent within 10% with masses estimated using a Kroupa (2001) or Chabrier (2003) IMF [2].

We present the results based on the visual classification and CAS (Conselice et al. 2000; Conselice 2003) parameters (§ 3) of GEMS F606W, rather than F850LP images, for the following reasons. The F606W images are ~ 1.2 AB magnitude deeper than the GEMS F850LP images and allow more reliable characterization of morphological features in the presence of cosmological surface brightness dimming at the rate of $(1+z)^{-4}$ (e.g., Barden et al. 2007). Furthermore, the low signal to noise in the F850LP images leads to large error bars on the asymmetry A and clumpiness S parameters generated by the CAS code, effectively making it impractical to use these values in CAS merger diagnostics (§ 3.4). When using the F606W images, we only include results over the redshift range $z \sim 0.24$–0.80 in order to ensure that the rest-frame wavelength λ_{rest} stays primarily in the optical band and does not shift well below the 4000 Å break. In the fourth redshift bin ($z \sim 0.6$ to 0.8) λ_{rest} shifts to the violet/near-UV (3700 Å to 3290 Å), but as we show in § 4.1, this does not significantly impact the results. We discard the last redshift bin at $z > 0.8$ where λ_{rest} shifts into the far-UV. In summary, based on the above considerations, we are left with a sample of ~ 4740 galaxies with $R_{\mathrm{Vega}} \leq 24$, over $z \sim 0.24$–0.80 ($T_{\mathrm{back}} \sim 3$–7 Gyr).

Figure 1 shows the rest-frame $U - V$ color plotted versus the stellar mass for this sample of ~ 4740 galaxies. The redshift interval is divided into four 1 Gyr bins. The diagonal line marks the separation of the red sequence and the blue cloud galaxies (BCG) at the average redshift z_{ave} of the bin. We use the definition in Borch et al. (2006) and Bell et al. (2004) for CDF-S:

---

[2]We adopt a Chabrier (2003) IMF when exploring the contribution of mergers to the cosmic SFR (§ 4.6 and § 4.7).

$$(U - V)_{\rm rest} > 0.227 \log({\rm M/M_\odot}) - 1.26 - 0.352z \tag{1}$$

The vertical lines on Figure 1 marks the mass completeness limit (Borch et al. 2006) for the red sequence galaxies. The blue cloud galaxies are complete well below this mass (Borch et al. 2006).

In this paper, we present results for two samples of astrophysical interest. The first sample (henceforth sample S1) focuses on galaxies with high stellar mass ($M \geq 2.5 \times 10^{10}$ $M_\odot$; Table 1). The sample size is originally 804 galaxies, out of which 798 (99.2%) could be visually classified. For this stellar mass range, the red sequence and blue cloud galaxies are both complete out to the highest redshift bin $z \sim 0.62$–0.80 for our sample, and we have theoretical predictions for comparison (see § 4.5) from semi-analytical models (e.g, Somerville et al. 2008; Hopkins et al. 2007; Khochfar & Burkert(2005); Bower et al. 2006), N-body (D'Onghia et al. 2008), and hydrodynamical SPH simulations (e.g., Maller et al. 2006). Note that the survey has few galaxies above 10^{11} $M_\odot$ (Fig. 1), and hence the high mass ($M \geq 2.5 \times 10^{10}$ $M_\odot$) sample primarily involves galaxies in the range 2.5×10^{10} to 10^{11} $M_\odot$.

We also present selected results for the sample S2 of ~ 3600 galaxies with $M \geq 1 \times 10^9$ $M_\odot$. Although this sample includes the ~ 790 high mass galaxies in sample S1, it is dominated by systems of intermediate mass ($10^9 \leq M/M_\odot < 2.5 \times 10^{10}$). Hence, we refer to sample S2 as the sample of intermediate mass galaxies. It consists of 3860 galaxies, of which 3698 ($\sim 96\%$) could be visually classified. We note that for the mass range $M \geq 1 \times 10^9$ $M_\odot$, the blue cloud is complete in our sample out to $z \sim 0.80$, while the red sequence is incomplete in the higher redshift bins. Where appropriate, we will therefore present results for the blue cloud sample only (e.g., lower part of Table 2).

3.   Methodology: Identifying Interacting and Non-Interacting Galaxies

3.1.   Overview of the Methodology

Galaxy mergers with a mass ratio $M1/M2 > 1/10$ can have a significant impact on galaxy evolution. According to simulations, major mergers (defined as those with mass ratio $1/4 < M1/M2 \leq 1/1$) typically destroy stellar disks, transforming them via violent relaxation, into systems with an $r^{1/4}$ de Vaucouleurs-type stellar profile, such as ellipticals (e.g., Negroponte & White 1983; Barnes & Hernquist 1991; Mihos & Hernquist 96; Struck 1997; Naab & Burkert 2001; but see Robertson et al 2004). These simulations suggest that ongoing/recent major mergers at $z \leq 1$ are associated with arcs, shells, ripples, tidal tails,

large tidal debris, highly asymmetric light distributions, double nuclei inside a common body, galaxies linked via tidal bridges of light, and galaxies enclosed within the same distorted envelope of light.

Minor mergers (defined as those with $1/10 < M1/M2 \leq 1/4$) of two spirals will not destroy the disk of the larger spiral (e.g., Hernquist & Mihos 1995; Smith et al. 1997; Jogee et al. 1999). Typically, the smaller companion sinks via dynamical friction, may excite warps, bars, spirals, and other non-axisymmetric perturbations, and leads to vertical heating, arcs, shells, ripples, tidal tails, tidal debris, warps, offset rings, highly asymmetric light distributions, etc (e.g., Quinn et al. 1993; Hernquist & Mihos 1995; Mihos et al. 1995; Quinn, Hernquist, & Fullagar 1993; Smith et al. 1994; Jogee 1999; Jogee et al. 1998, 1999; review by Jogee 2006 and references therein).

One goal of this paper is to identify strongly interacting systems, whose morphology and other properties suggest they are a recent merger of mass ratio $M1/M2 > 1/10$. As a guide to identifying these systems, we use the above morphological signatures seen in simulations. We employ two methods: a tailored visual classification system (§ 3.2) complemented with spectrophotometric redshifts and stellar masses, and a method based on quantitative asymmetry (A), and clumpiness (S) parameters (§ 3.4) derived using the CAS code (Conselice et al. 2000). While many studies use only automated methods or visual classification, we choose to use both methods in order to better assess the systematics, and to test the robustness of our results.

Our visually identified strongly interacting systems are candidates for a recent merger of mass ratio $M1/M2 > 1/10$. To further constrain galaxy evolution, it would be useful if we could separate these systems into major ($1/4 < M1/M2 \leq 1/1$) versus minor ($1/10 < M1/M2 \leq 1/4$) mergers. However, for many strongly interacting galaxies, it is not possible to unambiguously make this distinction, since the morphological disturbances induced depend not only on the mass ratio of the progenitors, but also on the orbital geometry (prograde or retrograde), the gas mass fraction, and structural parameters (e.g., Mihos & Hernquist 96; Struck 1997; Naab & Burkert 2001; Mihos et al. 1995, di Matteo et al. 2007). In effect, many signatures could be caused by both major and minor mergers. Thus, in § 3.3, we divide the strongly interacting systems into three categories: clear 'major merger', clear 'minor merger' and ambiguous 'major or minor' mergers. The first two categories allow us to set lower limits to the major and minor merger fraction.

3.2. Visual Classification of Galaxies as Interacting and Non-Interacting

We visually classified F606W images of the sample of ~ 4740 galaxies (§ 2) with $R_{\mathrm{Vega}} \leq$ 24 in the redshift range $z \sim 0.24$–0.80. A small subset (below 6%) of galaxies could not be classified due to image defects, low signal to noise, highly compact appearance, etc.

As described in § 3.1, the main goal of this paper is to identify strongly interacting candidates, which are likely candidates for a recent merger of mass ratio $M1/M2 > 1/10$. We use the morphological signatures suggested by the simulations outlined in § 3.1 to identify these systems and assign them the visual class of strongly interacting ('Int') galaxies. Figure 2 shows examples in the four 1 Gyr redshift bins. In practice, the class 'Int' of interacting galaxies consists of two sub-groups, 'Int-1' and 'Int-2', described below.

1. 'Int-1': A galaxy is assigned an 'Int-1' class if it exhibits a *strong morphological distortion*, such as a warped disk, an offset ring, arcs, shells and ripples, tidal tails, large tidal debris, very asymmetric light distributions, double nuclei inside a common body, and tidally distorted bridges of light. The basic idea here is that 'Int-1' galaxies are unambiguous cases of strongly interacting galaxies, since they exhibit the *morphological distortions induced by a strong gravitational disturbance*. Examples of 'Int-1' interacting systems are cases 3, 4, 5, 6, 7, 8, 9, 10, 11, and 12 in Fig. 2.

2. 'Int-2': A galaxy is assigned an 'Int-2' class if it is *fairly symmetric*, but has a companion, which satisfies three criteria: it is overlapping with it so that the two galaxies share a common envelope of light, making the pair be effectively a 'contact pair'; it has the same COMBO-17 spectrophotometric redshift within the accuracy $\delta_{\mathrm{z}}/(1 + z) \sim 0.02$ (§ 2); its stellar mass ratio satisfies $M1/M2 > 1/10$. The classification of a galaxy as an Int-2 contact pair depends on the accuracy of the spectrophotometric redshifts and stellar masses of both galaxies involved. We note here 'Int-2' contact pairs are less likely to be be line-of-sight chance projection than more distant pairs with $d \sim 20$ to 30 kpc. Examples of 'Int-2 interacting systems include both galaxies in case 7 of Fig 5, and the lower fairly symmetric galaxy in case 1 of Fig. 2. Most of our interacting systems fall in the class 'Int-1' rather than 'Int-2'.

Galaxies that show no evidence of an ongoing or recent merger of mass ratio $> 1/10$, according to the above-established criteria, are classified as 'Non-Interacting' galaxies. These galaxies may harbor very subtle distortions, but none of the type described in 'Int-1 and 'Int-2'. Galaxies in the class of 'Non-Interacting' consists of two sub-groups, 'Non-Interacting E-to-Sd' and 'Non-Interacting Irr1', which are shown in Figure 3, and described below.

1. 'Non-Interacting Irr1': It is important to note that even non-interacting galaxies have some inherent level of small-scale asymmetries in optical light due to SF activity. In

the case of low mass galaxies, further asymmetries may also arise due to the low ratio of rotational to random velocities, as is commonly seen in Im and Sm. These internally-triggered asymmetries due to SF in non-interacting galaxies differ in scale (few 100 pc vs several kpc) and morphology from the externally-triggered distortions typical of the 'Int-1' class. We classify non-interacting galaxies with such internally-triggered asymmetries as 'Irr1' (see Figure 3). Such systems may get accidentally picked as 'interacting' in automated asymmetry-based codes (see § 4.2).

2. 'Non-Interacting E-to-Sd': Galaxies are assigned the 'E to Sd' class if they are fairly symmetric, have Hubble types in the range E-to-Sd, and are not associated with any overlapping or contact companion.

In this paper, we are primarily concerned about the differences between three groups: the strongly interacting galaxies in class 'Int', the 'non-interacting E-to-Sd' galaxies, and the 'non-interacting Irr1' galaxies. The details of how 'E-to-Sd' galaxies are further sub-divided into individual Hubble types do not have any major impact on our main results, and we only describe this sub-classification for the sake of completeness. In the Hubble classification system (1936), as we go from E to Sd, the bulge to disk (B/D) luminosity ratio, as well as smoothness and tightness of any spiral arms, are expected to decrease. The Hubble system works fairly well on average in field galaxies, although it may fail in clusters (e.g., Koopmann & Kenney 1998). We use conventional definitions (Binney & Merrifield 1998) for individual Hubble types (E, S0, Sa, Sb-Sc, and Sd). We assign an elliptical (E) type if a galaxy exhibits a smooth featureless appearance, show no disk signatures, such as a bar or spiral arms, and appear to be pure spheroids. We assign an S0 class if a galaxy hosts a smooth central brightness condensation, surrounded by an outer component, which is relatively featureless (without spiral arms) and has a less steeply declining brightness profile (Binney & Merrifield 1998). We assign Sa, Sb-Sc, and Sd types using primarily visual estimates of the B/D ratio, and secondarily the smoothness/clumpiness of the disk. We do not accord much weight to the smoothness of spiral arms since the ACS F606W PSF ($\sim$ 260–560 pc at $z \sim 0.24$–0.80) precludes the identification of fine structures in the arms. In fact, at intermediate redshifts, where the faint smooth arms of Sa galaxies are not easily discernible, the distinction between E, S0, and Sa becomes blurred (see also § 4.1). However, this ambiguity between Es, S0s and Sas is not a problem for the subsequent analyses in this paper, since galaxies are grouped together either as 'E+S0+Sa' or 'E-to-Sd'.

The fraction of interacting, 'non-interacting E-to-Sd' galaxies, and ' non-interacting Irr1' galaxies is shown in Table 1 for the high mass sample, and in Table 2 for the intermediate mass sample. Further results and tests on the interaction history from visual classes are presented in § 4.1.

3.3.   Separating interacting galaxies into major and minor interactions

Our visually identified strongly interacting systems are candidates for a recent merger of mass ratio $M1/M2 > 1/10$. There are numerous astrophysical questions for which it would be useful to further separate these systems into major $(1/4 < M1/M2 \leq 1/1)$ versus minor $(1/10 < M1/M2 \leq 1/4)$ mergers. However, the morphological distortions induced in an interaction depend not only on the mass ratio $M1/M2$ of the progenitors, but also on the orbital geometry (prograde or retrograde), the gas mass fraction, and structural parameters (e.g., Mihos & Hernquist 96; Struck 1997; Naab & Burkert 2001; Mihos et al. 1995, Jogee 2006 and references therein; di Matteo et al. 2007).

In effect, many signatures could be caused by both major and minor interactions. Thus, we divide the strongly interacting systems into three categories: clear 'major merger', clear 'minor merger', and ambiguous 'major or minor merger' cases. The last category includes ambiguous cases that could be either major or minor, while the first two categories are clear cases of major and minor mergers, respectively. They allow us to set *lower limits* to the major and minor merger fraction.

The 'ambiguous/major or minor' merger category includes the following cases: a) Galaxies with double nuclei that are asymmetrically located, have different luminosities, and whose mass ratio is unknown as the system has only one single stellar mass based on COMBO-17 data (e.g., case 8 in Fig. 2). b) Systems with a morphological distortion that is strong, but not a 'train-wreck' (e.g., cases 3, 4, 5, 6, 7, 10, 11 in Fig. 2).

We assign a class of 'minor merger' to the following cases: (a) We include galaxies, which host an extended surviving disk with signs of a strong recent interaction, but do not have an overlapping companion of mass ratio $> 1/4$ with similar photometric redshift. The latter condition ensures that we do not capture the early phases of a major merger when the disks of the merging galaxies are starting to get distorted before they merge. The signs of strong interactions in the disk include a warp (e.g., case 2 in Fig. 2), prominent tidal debris and tails, and strong large-scale asymmetries. (b) We include galaxies (see § 3.2) with a companion that satisfies three criteria: it is overlapping or in contact so that the two galaxies share a common envelope of light; it has the same COMBO-17 spectrophotometric redshift within the accuracy $\delta_z/(1 + z) \sim 0.02$ (§ 2); and its stellar mass ratio satisfies $(1/10 \leq M1/M2 < 1/4)$. Such minor mergers are in progress (e.g., case 2, 4 in Fig. 2).

We assign a class of 'major merger' to the following cases: (a) Galaxies with extremely distorted 'train-wreck' morphologies. (b) Galaxies with double nuclei that are symmetrically located and have comparable luminosities (e.g., case 6, 12 in Fig. 2). (c) Galaxies with a companion that satisfies three criteria: it is overlapping or in contact so that the two galaxies

share a common envelope of light; it has the same COMBO-17 spectrophotometric redshift within the accuracy $\delta_z/(1 + z) \sim 0.02$ (§ 2); and its stellar mass ratio satisfies ($M1/M2 > 1/4$). Such major mergers are in progress (e.g., case 1 with a stellar mass ratio $\sim 1/4$ in Fig. 2).

The fraction of interacting galaxies, and their subdivision into the classes 'minor', 'major', and 'major or minor' mergers are shown in Table 1 for the high mass sample, and in Table 2 for the intermediate samples. The results are further discussed in § 4.3.

3.4. CAS

We derived the concentration C, asymmetry A, and clumpiness S (CAS) parameters by running the the CAS code (Conselice et al. 2000) on the F606W images. As is standard practice, the segmentation maps produced during the original source extraction (Caldwell et al. 2008) are used to mask neighbors on each ACS tile. The CAS code derives the asymmetry index A (Conselice 2003) by rotating a galaxy image by 180 deg, subtracting the rotated image from the original image, summing the absolute intensities of the residuals, and normalizing the sum to the original galaxy flux. CAS improves the initial input center with the IRAF task 'imcenter' and then performs a further refinement within a 3×3 grid, picking the center that minimizes A. The CAS concentration index C (Bershady et al. 2000) is proportional to the logarithm of the ratio of the 80% to 20% curve of growth radii within 1.5 times the Petrosian inverted radius at $r(\eta = 0.2)$, normalized by a logarithm

$$C = 5 \times \log(\mathrm{r}_{80\%}/\mathrm{r}_{20\%}) \tag{2}$$

The clumpiness index S (Conselice 2003) is defined as the ratio of the amount of light contained in high-frequency structures to the total amount of light in the galaxy. In order to compute S, the CAS code first smooths the galaxy image with a filter of size equal to 1/6 of the Petrosian radius to produce a lower resolution image whose high-frequency structure has been washed out. The latter image is then subtracted from the original image to produce a residual map that contains only the high-frequency components of the galaxy's stellar light. The flux of this residual light is then summed and divided by the sum of the original galaxy image flux to obtain a galaxy's clumpiness (S) value. Tests on the interaction history from CAS are presented in § 4.2.

It has been argued that the criterion $A > 0.35$ and $A > S$ (henceforth referred to as the CAS merger criterion) captures galaxies that exhibit large asymmetries produced by major mergers (Conselice 2003). We will assess this in § 4.2.

4. Results and Discussion

4.1. The interaction fraction from visual classes

Fig 4 compares the fraction (f) of strongly interacting galaxies, for both the high mass ($M \geq 2.5 \times 10^{10}$ $M_\odot$) and intermediate mass ($M \geq 1 \times 10^9$ $M_\odot$) sample, based on visual classification by 3 classifiers (SJ, SM, KP). On this figure, the plotted error bar for f only includes the binomial term $[f(1\text{-}f)/N]^{1/2}$, for each bin of size N. The same trend is seen for all 3 classifiers and the maximum spread $\delta_{\rm f}/f$ in the 4 bins is 15%, 17%, 26% and 26%, respectively. In subsequent analyses, we adopt an error bar on f that includes in quadrature both the binomial term and a dispersion of 26% to capture the inherent subjectivity in the visual classification.

Another key test is to assess the impact of redshift-dependent systematic effects, such as bandpass shifting. When using the F606W filter whose pivot wavelength is ~ 5915 Å, the rest frame wavelength ($\lambda_{\rm rest}$) corresponds to the rest-frame optical at the mean redshift of the first 3 bins, but shifts to the rest-frame violet/near-UV (3700 Å to 3290 Å) in the last bin ($z \sim 0.6$ to 0.8). Galaxies tend to look slightly more asymmetric at near-UV wavelengths due to the prominence of young stars. In order to quantitatively test the impact of bandpass shift on our visual classes, we use the redder F850LP images from the GOODS survey, which overlaps with the central 20% of the GEMS survey area. The F850LP filter has a pivot wavelength of 9103 Å and traces the rest-frame optical (7340 Å to 5057 Å) in all four redshift bins out to $z \sim 0.8$. They also have 5 times longer exposures than the GEMS F850LP and F606W images. Fig 5 shows GEMS F606W and GOODS F850LP images of typical disturbed and normal galaxies in the last 2 redshift bins ($z \sim 0.47$ to 0.8).

While the GOODS images have higher S/N, and trace redder older stars, they do not reveal dramatically different morphologies from those in the GEMS F606W images (Fig 5). Furthermore, the 855 intermediate mass ($M \geq 1 \times 10^9$ $M_\odot$) galaxies in the GEMS/GOODS overlap area, were classified using both GOODS F850LP and GEMS F606W images by the 3 classifiers. We find that the ratio of ($f_{\rm GEMS}/f_{\rm GOODS}$) ranges from 0.8 to 1.2 across the 3 classifiers (Table 3), where $f_{\rm GEMS}$ and $f_{\rm GOODS}$ are the fraction of strongly interacting galaxies based on the GEMS F606W and GOODS F850LP images, respectively. The mean f changes by only 6% (Table 3). In effect, over 85% of the galaxies classified as disturbed ('Int') in the GEMS F606W images retain the same visual class in the GOODS F850LP. Among the remaining objects, some classified as 'Non-Interacting' in GEMS F606W get reclassified as disturbed in GOODS F850LP, and vice-versa The fact that f does not change by a large amount between GEMS F606W and GOODS F850LP is not surprising, since the rest-frame wavelength of GEMS F606W in the last bin shifts only to the violet/near-UV, rather than to

the far-UV, where morphological changes are more dramatic. We conclude that our results are not highly impacted by bandpass shifting, and any effect is accounted for by our error bars of $> 26\%$ in f.

Another redshift-dependent systematic effect is surface brightness dimming at the rate of $(1+z)^{-4}$ (e.g., Barden et al. 2008). This leads to surface brightness dimming by a factor of 1.0 to 2.5 magnitude over the redshift range 0.24 to 0.80. This is mitigated in part by two factors: galaxies are on average 1.0 magnitude brighter in surface brightness by $z \sim 0.8$ (e.g., Barden et al. 2005), and the average SFR rises by a factor of ~ 4 out to $z \sim 0.8$ (e.g., see § 4.6). Two approaches can be adopted to assess the impact of surface brightness dimming. The first is to artificially redshift strongly disturbed galaxies in the lowest redshift bin ($z \sim 0.24$) out to $z \sim 0.8$, either assuming passive evolution or adding in a ~ 1 magnitude of brightening in surface brightness. However, this approach suffers from the limitation that it implicitly assumes that galaxies at $z \sim 0.8$ are similar to those at $z \sim 0.24$ and evolve passively with time. A better approach, which does not make such assumptions, is to repeat the analysis and visual classification using *deeper* images of the galaxies and assess the resulting change in visual classes. The above-described test performed using the deep GOODS F850LP image (Fig. 5) is an example of such a test.

Finally, as an extra test, we checked the distribution of Sérsic indices n for single-component Sérsic fits (Barden et al. 2005) for the visual classes of the sample S2 of intermediate mass $M \geq 1 \times 10^9$ $M_\odot$ galaxies (Fig. 6). Non-interacting disk-dominated systems are expected to have $n < 2.5$, while massive ellipticals and bulge-dominated systems typically have higher Sérsic indices. We indeed find that over 85% of the systems visually classified as Sb-Sd and Irr have $n < 2.5$ in the intermediate mass ($M \geq 1 \times 10^9$ $M_\odot$) sample. The systems typed as ellipticals (E) have mostly $n > 3$, and as expected, their distribution peaks at $n \sim 4$, corresponding to a de Vaucouleurs profile. The types S0 and Sa have n values bridging those of the E and disk (Sb-Sc and Sd-Irr) systems. Most of them have $n < 3$, but there is a long tail of S0s and Sas with higher n. This is expected given the previously described (§ 3.2) difficulties in separating E, S0, and Sa galaxies at intermediate redshifts. However, this ambiguity between types E, S0 and Sa is not a problem for the subsequent analyses in this paper, since galaxies are grouped together either as 'E+S0+Sa' or 'E-to-Sd'. In fact, as stressed in § 3.2, the main results presented in this paper depend only on the differences between three groups: strongly interacting galaxies ('Int'),'Non-Interacting E to Sd', and 'Non-Interacting Irr1'.

4.2. The interaction fraction from CAS

It has been argued that the CAS merger criterion ($A > 0.35$ and $A > S$) captures galaxies that exhibit large asymmetries produced by major mergers (Conselice 2003). This criterion is based on calibrations of the CAS system (Conselice et al. 2000) at optical rest-frame wavelengths ($\lambda_{\mathrm{rest}} > 4500\,\text{Å}$). However, there are several caveats: a) The CAS criterion ($A > 0.35$ and $A > S$) will miss out strongly interacting galaxies where the morphological distortions contribute to less than 35 % of the total galaxy flux. (b) Calibrations of A with N-body simulations (Conselice 2006) shows that during major mergers with mass ratios 1:1 to 1:3, the asymmetry oscillates with time. Typically, it exceeds 0.35 for ~ 0.2 Gyr in the early phases when the galaxies start to interact, falls to low values as the galaxies separate, rises for ~ 0.2 Gyr as they approach again for the final merger, and eventually tapers down as the final remnant relaxes. On average, the $A > 0.35$ criterion is only satisfied for one third of the merger timescale in these N-body simulations. For minor mergers of mass ratios 1:5 and below, the asymmetries are too low to satisfy $A > 0.35$. (c) To complicate matters, automated asymmetry parameters can also capture non-interacting galaxies whose visible light shows small-scale asymmetries due to star formation (e.g., Miller et al. 2008)

Visual tests that verify how well the CAS criterion ($A > 0.35$ and $A > S$) works at intermediate redshifts have been performed using spot checks and small-to-moderate samples (e.g., Mobasher et al 2004; Conselice 2003; Conselice et al. 2003; Conselice et al. 2005). However, what has been missing to date is a quantitative estimate, based on a large sample of galaxies, of the recovery fraction of CAS (i.e., the fraction of visually-classified interacting galaxies that the CAS criterion picks up), and the contamination level of CAS (i.e., the fraction of visually-classified non-interacting galaxies that the CAS criterion picks up). Both the recovery fraction and contamination level might be expected to depend on the rest-frame wavelength used, the mass and SFR of the galaxies, etc. In this paper, we perform one of the most extensive comparisons to date, at intermediate redshifts ($z \sim 0.24$ to 0.80), between CAS-based and visual classification results for both high mass ($M \geq 2.5 \times 10^{10}\ M_\odot$) and intermediate mass ($M \geq 1 \times 10^9\ M_\odot$) galaxies. We assess the effectiveness of the CAS merger criterion ($A > 0.35$ and $A > S$) over this interval, where the rest-frame wavelength λ_{rest} varies from 4770 Å to 3286 Å. We note that the rest-frame wavelength range here extends to somewhat bluer wavelengths than the range ($\lambda_{\mathrm{rest}} > 4500$ Å) over which the CAS system was calibrated.

Fig 4 compares the interaction fractions that would be obtained using the CAS criterion (f_{CAS}), as opposed to visual classification (f). For the high mass ($M \geq 2.5 \times 10^{10}\ M_\odot$) galaxies, visually based and CAS-based interaction fractions agree within a factor of two, with f being higher than f_{CAS} at $z < 0.5$, and being lower at $z > 0.5$ (top panel of Fig 4).

However, for the intermediate mass ($M \geq 1 \times 10^9$ $M_{\odot}$) galaxies (lower panel of Fig 4), at $z > 0.5$ the CAS-based interaction fraction can be systematically higher by a factor ~ 3 than the visually based f. The reason for this discrepancy, as we show below, is that at bluer rest-frame wavelengths (i.e., higher redshifts), the CAS criterion picks up a significant number of non-interacting dusty, star-forming galaxies.

Fig. 7 plots the CAS asymmetry A and clumpiness S parameter for galaxies in the four redshift bins covering the interval $z \sim 0.24$–0.80. Galaxies satisfying the CAS criterion ($A > 0.35$ and $A > S$) lie in the upper left hand corner, bracketed by the $A = S$ and $A = 0.35$ lines. One can see that while the CAS criterion captures a fair fraction of the strongly interacting galaxies (coded as orange stars), it also picks up a large number of non-interacting galaxies.

This is further illustrated in Fig. 8. The top panel show the recovery fraction of CAS, defined as the fraction of the visually-classified strongly interacting galaxies ('Int') picked up by the CAS criterion ($A > 0.35$ and $A > S$). For the intermediate mass ($M \geq 1 \times 10^9$ $M_{\odot}$) sample, only $\sim$ 50% to 70% of the visually classified interacting galaxies satisfy the CAS criterion across the four redshift bins. We inspected the systems missed out by the CAS criterion ($A > 0.35$ and $A > S$) and show typical cases in the top panel of Fig. 9. The missed cases include pairs of relatively symmetric galaxies with similar spectrophotometric redshifts and mass ratio $M1/M2 > 1/10$ (e.g., case 1 in Fig. 9); galaxies where the tidal features and small accreted satellite in the main disk of a galaxy (e.g., case 3 in Fig. 9) likely contribute less than 35% of the total light; and galaxies with close double nuclei (e.g., case 2 in Fig. 9), where CAS might refine the center to be between the two nuclei, thereby leading to a low $A < 0.35$.

The lower panel of Fig. 8 illustrates the large contamination level of the CAS system. N_{CAS} represents the number of galaxies satisfying the CAS criterion ($A > 0.35$ and $A > S$) in the four redshift bins. The majority (44% to 80%) of these systems turn out to be 'Non-Interacting E-Sd' and 'Non-Interacting Irr1' galaxies. Typical cases are shown in the lower panel of Fig. 9. They include non-interacting actively star-forming systems where SF induces small-scale asymmetries in the optical blue light (e.g., cases 4 and 6 in Fig. 9); systems where A is high due to the absence of a clearly defined center (e.g., case 8 in Fig. 9) or due to the center being blocked by dust (e.g., cases 4 and 9 in Fig. 9); galaxies whose outer parts look irregular (e.g., cases 7 and 8 in Fig. 9); and edge-on systems and compact systems, where the light profile is steep such that small centering inaccuracies can lead to large A (e.g., case 9 in Fig. 9).

In summary, we find that the CAS-based interaction fraction agrees within a factor of two with visually based one for high mass ($M \geq 2.5 \times 10^{10}$ $M_{\odot}$) galaxies, but can overestimate

the interaction fraction at $z > 0.5$ by a factor ~ 3 for intermediate mass ($M \geq 1 \times 10^9\ M_\odot$) galaxies. For the latter mass range, the systems counting toward f_{CAS} are a mixed bag: the CAS criterion misses about half of the visually-classified strongly interacting galaxies, but picks up a dominant number of non-interacting dusty, star-forming galaxies. We thus conclude that the CAS merger criterion is ill-suited for use on *HST V*-band images at $z > 0.5$, where the rest frame wavelength falls below $\lambda < 4000$ Å, particularly in the case of intermediate mass galaxies with significant SF, gas, and dust. Modified CAS criteria in the near-UV based on morphological k-corrections (Taylor et al. 2007) might alleviate this problem.

4.3. Interaction history of massive and intermediate mass galaxies

Based on the tests in § 4.1 and § 4.2, we decided to adopt the mean interaction fraction f based on visual classes for our two samples of interest. Results are shown in Table 1 for the high mass ($M \geq 2.5 \times 10^{10}\ M_\odot$) sample, which is complete on both the blue cloud and red sequence (§ 2). The error bar shown on f in both tables now includes the sum in quadrature of a binomial term $[f(1\text{-}f)/N]^{1/2}$ for each bin of size N, along with a fractional error of $\pm 26\%$ to capture the dispersion between classifiers, and uncertainties due to bandpass shifting and surface brightness dimming.

From Table 1 and Fig 4, it can be seen that the fraction f of strongly interacting systems among high mass ($M \geq 2.5 \times 10^{10}\ M_\odot$) galaxies remains fairly constant over lookback times of 3–7 Gyr, ranging from $9\% \pm 5\%$ at $z \sim 0.24$–0.34, to $8\% \pm 2\%$ at $z \sim 0.60$–0.80, as averaged over every Gyr bin. As discussed in § 3.1, these systems appear to be in late or post-merger phases, and are candidates for a recent merger of mass ratio $M1/M2 > 1/10$.

As outlined in § 3.3, the interacting galaxies were divided among 3 classes: clear 'major merger', clear 'minor merger', and ambiguous 'major or minor merger' cases, and the first two classes were thereafter used to set lower limits on the major and minor merger fraction. The lower limit on the major ($M1/M2 > 1/4$) merger fraction, determined in this way, ranges from 1.1% to 3.5% over $z \sim 0.24$–0.80. The corresponding lower limit on the minor ($1/10 \leq M1/M2 < 1/4$) merger fraction ranges from 3.6% to 7.5%. The ambiguous cases of 'major or minor merger' make up a fraction between 1.2% to 2.0%. To our knowledge, this is the first, albeit approximate, empirical estimate of the frequency of minor mergers over the last 7 Gyr. It provides an important constraint since minor mergers dominate the merger rates in ΛCDM models.

When converting the observed fraction f of galaxy mergers into a merger rate R, we

must bear in mind that in any observational survey of galaxies, mergers can only be recognized for a finite time t_{vis}, which is the timescale over which a merging galaxy will appear morphologically distorted. This timescale depends on the mass ratio of the merger as well as the gas fraction of the progenitors: $t_{\text{vis}} \sim 0.5$ 0.8 for gas-rich galaxies, and $t_{\text{vis}} \sim 0.2$–0.4 Gyr for gas-poor galaxies (T.J. Cox, private communication). This timescale will also depend on many observational factors such as the method used to identify mergers (e.g. visual classification vs. CAS or other statistical methods) and the depth of the imaging used. We assume a representative value of $t_{\text{vis}} = 0.5$ Gyr here, but we must keep in mind that there are at least factors of two uncertainty in this number. The merger rate R is given by

$$R = \frac{n\ f}{t_{\text{vis}}}, \tag{3}$$

where n is the comoving number density of galaxies above a certain mass limit in the redshift bin. For our measured merger fraction and assumed value of $t_{\text{vis}} \sim 0.5$ Gyr, the corresponding merger rate R is a few $\times 10^{-4}$ galaxies Gyr^{-1} Mpc^{-3} (Fig. 11). It also follows that for an assumed visibility time of ~ 0.5 Gyr, each massive galaxy has on average undergone $f/t_{\text{vis}} \sim 0.17$ mergers of mass ratio $> 1/10$ per Gyr, or ~ 0.7 mergers of mass ratio $> 1/10$ over the redshift interval $z \sim 0.24$–0.80 ($T_{\text{back}} \sim 3$–7 Gyr). *Of these ~ 0.7 mergers of mass ratio $> 1/10$, we estimate that 0.2 are major mergers, ~ 0.4 are minor mergers, and ~ 0.1 are ambiguous cases of either major or minor mergers.*

At intermediate masses ($M \geq 1 \times 10^9\ M_\odot$) where we are only complete in mass for the blue cloud (§ 2), we consider f to be meaningful only for the intermediate mass blue cloud sample. Results for this sample are shown in the lower part of Table 2. The fraction of blue cloud galaxies having undergone recent mergers of mass ratio $> 1/10$ ranges from $7\% \pm 2\%$ to $15\% \pm 5\%$ over $z \sim 0.24$–0.80. The corresponding merger rate R ranges from 8×10^{-4} to 1×10^{-3} galaxies Gyr^{-1} Mpc^{-3} . For an assumed visibility time of ~ 0.5 Gyr, it follows that over $z \sim 0.24$–0.80 ($T_{\text{back}} \sim 3$–7 Gyr), each intermediate mass blue cloud galaxy has on average undergone 0.84 mergers of mass ratio $> 1/10$, of which an estimated 0.05 are major mergers, 0.22 are minor mergers, and 0.57 are ambiguous cases of either major or minor mergers.

4.4. Comparison with other studies

When comparing our observed fraction f of strongly interacting galaxies in the high mass ($M \geq 2.5 \times 10^{10}\ M_\odot$) sample over $z \sim 0.24$–0.80 with published studies, several caveats must be borne in mind. Many studies have small samples and large error bars at $z < 0.8$ (e.g., Conselice 2003; Fig. 10). Others focus on bright galaxies and luminosity-selected samples

(e.g., Lotz et al. 2008; Casatta et al. 2005) rather than stellar mass selected sample, because the data to derive stellar masses were unavailable. Different studies target different systems, ranging from morphologically distorted galaxies to close pairs with separation $d \sim 5$ to 30 kpc. Finally, many studies focus only on major mergers, while the strongly interacting galaxies identified in our study are candidates for a merger of mass ratio $M1/M2 > 1/10$ (§ 3.1), and include both minor and major mergers. Nonetheless, we attempt approximate comparisons.

Fig. 10 shows the the fraction f_{Gini} of morphologically disturbed systems based on Gini-M20 parameters among $M_{\mathrm{B}} < $ -20.5 and $L_{\mathrm{B}} > 0.4\ L_*$ galaxies in the Extended Groth Strip (Lotz et al. 2008). The latter study does not present any results for a high mass sample, and thus we effectively are comparing their bright galaxies to our high mass galaxies. Over $z \sim$0.2–0.80, our results are in very good agreement, within a factor of less than two, with f_{Gini}. The CAS-based results from Conselice (2003) are derived from a small sample in the Hubble Deep Field and have error bars that are too large to set useful constraints at $z < 1$ (Fig. 10). Our results of a fairly flat evolution of the merger rate out to $z \sim 0.8$ also agree with the results of Cassata et al. (2005), based on both pairs and asymmetries.

What about studies based on close pairs? The major merger fraction of massive galaxies ($M_* \geq 2.5 \times 10^{10}\ M_{\odot}$) in close ($d < 30$ kpc) pairs, based on the 2-point correlation function in COMBO-17, is $5\% \pm 1\%$ averaged over at $0.4 < z < 0.8$ (Bell et al. 2006). This value is lower than our fraction f ($\sim 8\% \pm 2\%$) of interacting galaxies, which represent likely mergers of mass ratio $> 1/10$, and it is higher than the fraction of cases we see as clear major mergers ($\sim 1.3\% \pm 0.2\%$). The study of luminous ($L_{\mathrm{V}} > 0.4\ L_*$) pairs at projected separations of 5–20 kpc in the COSMOS field (Kartaltepe et al. 2007) finds a galaxy pair fraction of $\sim 1\%$–3% over $z \sim 0.24$–0.80, corresponding to a galaxy merger fraction of $\sim 2\%$–6% . Our observed fraction f of $9\% \pm 5$ to $8\% \pm 2\%$ over $z \sim 0.24$–0.8 is slightly higher and flatter than this study.

The differences we see through these comparisons are already known (see § 1). Studies based on close pairs tend to show fairly strong evolution in the major merger rate out to $z \sim 1$ (e.g., Kartaltepe et al 2007; Bell et al 2006; Lin 2004), while studies based on asymmetries (e.g., Lotz et al. 2008; this study), and studies based on both pairs and asymmetries (Cassata et al. 2005) tend to report a fairly flat evolution of the merger rate with redshift up to z$\sim$ 1. It is not fully understood why these three different methods yield different results. Part of the difference could be due to the methods tracing different phases of an interaction, with the pair method tracing the potential pre-merger phase, while the method based on the distorted galaxies trace the later phases, including the merging and post-merging phases.

Another point is that both pair and asymmetry methods are imperfect ways of tracing

the merger fraction. Methods tracing morphologically disturbed galaxies may capture some fly-by tidal interactions rather than mergers, and this effect would cause the fraction of strongly interacting galaxies to overestimate the merger fraction. However, this effect is not a dominant one for the following reason: interaction signatures typically persist for a visibility timescale of 0.5 Gyr (T_{vis}), and a fly-by companion causing the distortion would still be within 100 kpc of the disturbed galaxy, assuming an escape speed of 200 km/s. The distorted galaxies we identify do not typically have such a fly-by companion, of mass ratio $> 1/10$ and similar spectrophotometric redshift. In studies based on close pairs, one source of uncertainty is that even pairs with members at the same redshift may not become gravitationally bound in the future. This effect might cause pairs to overestimate the true major merger fraction. On the other hand, erroneous spectrophotometric redshifts can cause us to either overestimate or underestimate the true close pair fraction, with the latter effect being more likely. Corrections for this effect are uncertain and depend on the shape of the spectrophotometric redshift errors (e.g., see Bell et al. 2006 for discussion).

4.5.   Comparison of interaction history with ΛCDM simulations

We compare our empirical merger rate R (Fig. 11) to predictions from different theoretical models of galaxy evolution in the context of a ΛCDM cosmology, including the halo occupation distribution (HOD) models of Hopkins et al. (2007); semi-analytic models (SAMs) of Somerville et al. (2008), Bower et al. (2006), and Khochfar & Silk (2006); and the cosmological smoothed particle hydrodynamics (SPH) simulations from Maller et al. (2006). The models were provided to us directly by the authors or co-authors of these individual studies.

We first briefly describe the general problem of calculating galaxy merger rates. Predicting the rate of mergers per comoving volume and per unit time between *isolated* dark matter (DM) halos within a ΛCDM model is relatively straightforward via semi-analytic methods or N-body simulations (e.g. Lacey & Cole 1993; Gottlöber et al. 2001; Fakhouri & Ma 2008; Neistein & Dekel 2008; D'Onghia et al. 2008). However, making a direct prediction of the *galaxy* interaction rates is more complicated due to a number of factors, including the difference between the galaxy and halo merger timescales, tidal heating and stripping of halos and sub-halos, the effect of a dense core of baryons on merging satellites, and the non-linear relation at low mass between DM halo (or sub-halo) mass and galaxy mass (van den Bosch et al. 2007). Thus, attempts to extract a *galaxy* merger rate from ΛCDM simulations also must attempt to model the relationship between dark matter and galaxy properties. The three main methods for making this connection are HOD models, SAMs, and hydrodynamic

simulations. We summarize below how these the three types of models differ.

HOD models specify the probability that a DM halo of a given mass M harbors N galaxies above a given mass or luminosity. The parameters of this function are determined by requiring that statistical observed quantities, such as galaxy mass or luminosity functions and galaxy correlation functions, be reproduced. The merger rate of galaxies within their host halos is calculated via standard or improved dynamical friction formulae. In the HOD models of Hopkins et al. (2007) used here, different modified formulae can be used, which include the effect of a gravitational capture cross section, stripping of DM halos, and calibration factors from N-body simulations. The predicted model rate can vary by a factor of ~ 2 depending on model assumptions for sub-halo structure and mass functions, the halo occupation statistics, and the dynamical friction formulae used.

In SAMS, merger trees of DM halos are either extracted from cosmological N-body simulations or derived using analytic methods (e.g., Somerville & Kolatt 1999). Calibrated modified versions of the Chandrasekhar dynamical friction approximation (e.g. Boylan-Kolchin et al. 2008) are used to compute the galaxy merger rate. Simplified analytic formulae are used to model the cooling of gas, star formation, supernova feedback, and more recently, AGN feedback (e.g., Somerville et al. 2008; Bower et al. 2006; Croton et al. 2006; Benson et al. 2005; Cole et al. 2000; Somerville & Primack 1999). The free parameters in these formulae are normalized to reproduce observations of nearby galaxies, such as the $z = 0$ galaxy mass or luminosity function. Fig. 11 shows results of three independent SAMs from Khochfar & Silk (2006), Bower et al. (2006), and Somerville et al. (2008).

Cosmological hydrodynamic simulations attempt to model the detailed physics of gas hydrodynamics and cooling as well as gravity by explicitly solving the relevant equations for particles or grid cells. SPH methods are most commonly used. SF and supernova feedback are treated using empirical recipes. A drawback of this approach is that, due to computational limitations, state-of-the-art simulations still do not have the dynamic range to resolve the internal structure of galaxies while simultaneously treating representative cosmological volumes. Another well known problem is that cosmological SPH models, which do not include some kind of suppression of cooling in massive halos (e.g., due to AGN feedback) do not reproduce the observed number density of galaxies on the mass scales of interest (few $\times 10^{10} M_\odot$). Thus, the simulations of Maller et al. (2006) shown here, over-predict the number of high mass and low mass galaxies, while galaxies at the bend of the Schechter mass function are a factor of 2 to 3 too massive. In order to make the simulated mass function agree better with observations, Maller et al. (2006) apply a correction factor of 2.75 for galaxies in the mass range $2 \times 10^{10} < M_*/M_\odot < 6 \times 10^{11}$. This correction is already included in the model on Fig. 11.

When comparing the observations to the models, one must consider carefully how merger rates are determined in these simulations. Two approaches are used: one based on simulation snapshots and the other based on a light cone. In the first approach, simulation outputs ("snapshots") are stored at a sequence of redshifts. By considering two snapshots separated by a time Δt and counting the number of N_{mrg1} of galaxies that have undergone a merger of a given mass ratio $M1/M2$ over Δt, one can determine the merger rate using $R_{\mathrm{mod1}} = N_{\mathrm{mrg1}}/(\Delta t \, V)$, where V is the comoving volume of the simulation box. Only galaxies above a certain mass cut are considered and the same cut ($M_* \geq 2.5 \times 10^{10}$) used in the data is applied to the simulations. When comparing the simulations to the observations averaged over a given redshift bin defined by lookback times t_{hi} and t_{lo}, the models try to mimic the observations as closely as possible by picking the two snapshots to be at t_{hi} and t_{lo}. Except for Somerville et al (2008), all the models presented on Fig. 11 derive the merger rate R using the above approach, based on simulation snapshots

For the Somerville et al. (2008) models, the simulation analysis was carried out in a way that is closer to the observations. We construct a light cone with a geometry that is equivalent to three GEMS fields (2700 arcmin^2 from $0.1 < z < 1.1$). We then divide the galaxies into redshift bins, exactly as in the observational analysis, and we count the number N_{mrg2} of galaxies that have had a merger within a time t_{vis} in the past. These galaxies appear as morphologically distorted mergers in the observations. The model merger fraction is $f_{\mathrm{mod2}} = N_{\mathrm{mrg2}}/N_{\mathrm{gal2}}$, where N_{gal2} is the total number of galaxies above the relevant mass limit in this light cone or redshfit bin. The model merger rate is calculated exactly as in the data using using $R_{\mathrm{mod2}} = f_{\mathrm{mod2}} \, n_{\mathrm{mod2}}/t_{\mathrm{vis}}$, where n_{mod2} is the comoving number density of galaxies above a certain mass limit in the redshift bin. Note that N_{mrg2} and f_{mod2} are quite sensitive to t_{vis}, while R is independent of t_{vis}.

In Fig. 11, we compare our empirical results to the model merger rate R_{mod1} and R_{mod2}. In both data and models, major and minor mergers are defined as those with mass ratio ($M1/M2 > 1/4$), and ($1/10 \leq M1/M2 < 1/4$), respectively. The only slight exception is in the case of Maller et al (2006) model where the extracted major mergers were defined with a slightly lower mass cutoff ($M1/M2 > 1/3$). The dotted lines on Fig. 11 show the major merger rate for all the models. The solid line show the (major+minor) merger rate, in other words, the rate of mergers with mass ratio ($M1/M2 > 1/10$). This is shown for all models except the Maller et al (2006) SPH simulations, where the limited dynamic range of the current simulations only allows predictions for major mergers. The solid line can be directly compared to our empirical merger rate R (§ 4.3 equation (3)), since the latter is based on galaxies that are likely mergers of mass ratio $M1/M2 > 1/10$.

We find qualitative agreement between the observations and models, with the (ma-

jor+minor) merger rate from different models (solid lines) bracketing the observed rate (stars) on Fig. 11, and showing a factor of five dispersion. One can now anticipate that in the near future, improvements in both the observational estimates and model predictions will start to rule out certain merger scenarios and refine our understanding of the merger history of galaxies.

4.6.   The impact of galaxy interactions on the average SFR over the last 7 Gyr

The idea that galaxy interactions trigger strong star formation in galaxies is known from observations (e.g., Larson & Tinsley 1978; Joseph & Wright 1985; Kennicutt et al. 1987; Barton et al 2003) and simulations (e.g., Negroponte & White 1983; Hernquist 1989; Barnes & Hernquist 1991, 1996; Mihos & Hernquist 1994, 1996; Springel, Di Matteo & Hernquist 2005). However, simulations cannot uniquely predict the factor by which interaction enhance the SF activity of galaxies over the last 7 Gyr, since both the SFR and properties of the remnants in simulations are highly sensitive to the stellar feedback model, the bulge-to-disk (B/D) ratio, the gas mass fractions, and orbital geometry (e.g., Cox et al 2006; di Matteo et al. 2007). Thus, we explore here the impact of interactions on the average UV-based and UV+IR-based SFR of intermediate-to-high mass ($M \geq 1 \times 10^9 \ M_\odot$) galaxies over $z \sim 0.24$–0.80.

We adopt the SFRs in Bell et al. (2005, 2007), based on COMBO-17 UV data (Wolf et al. 2004) and deep Spitzer 24 μm observations with a limiting flux of $\sim 83 \ \mu$ Jy (5σ) from the Spitzer Guaranteed Time Observers (Papovich et al. 2004; Gordon et al. 2005). The unobscured SFR based on the directly observable UV light from young stars was computed using $\mathrm{SFR_{UV}} = 9.8 \times 10^{-11}$ (2.2 L_{UV}), where $L_{\mathrm{UV}} = 1.5\nu l_{\nu,2800}$ is a rough estimate of the total integrated 1216–3000 Å UV luminosity, derived using the 2800 Å rest-frame luminosity from COMBO-17 $l_{\nu,2800}$. The factor of 1.5 used in converting the 2800 Å luminosity to total UV luminosity accounts for the UV spectral shape of a 100 Myr-old population with constant SFR. The factor of 2.2 corrects for the light emitted longward of 3000 Å and shortward of 1216 Å. The SFR calibration is derived from Pégase assuming a 100 Myr old stellar population with constant SFR and a Chabrier (2003) IMF.

The obscured SFR can be calculated from dust-reprocessed IR emission using the expression $\mathrm{SFR_{IR}} = 9.8 \times 10^{-11} \ L_{\mathrm{IR}}$, where L_{IR} is the total IR luminosity (TIR) over 8–1000 μm. L_{IR} is constructed from the observed 24 μm flux (corresponding to rest-frame wavelengths of 19–13 μm over $z \sim 0.24$–0.80) using the method outlined in Papovich & Bell (2002), based on an average Sbc template from the Devriendt et al. (1999) SED library. In converting from L_{IR} to $\mathrm{SFR_{TIR}}$, Bell et al. (2007) assume that the bulk of the 24 μm emission comes

from SF, and not from AGN activity, based on the statistical result that less than 15% of the total 24 μm emission at $z < 1$ is in X-ray luminous AGN (e.g., Silva et al. 2004; Bell et al. 2005; Franceschini et al. 2005; Brand et al. 2006). Uncertainties in these SFR estimates are no less than a factor of 2 for individual galaxies while the systematic uncertainty in the overall SFR scale is likely to be less than a factor of 2 (Bell et al. 2007).

We investigate the star formation properties of the sample S2 of $\sim$3698 intermediate mass ($M \geq 1.0 \times 10^9 \ M_\odot$) galaxies. This sample is complete for the blue cloud, but incomplete for the red sequence in the highest redshift bins (§ 2). However, since most of the SFR density originates from the blue cloud, this incompleteness does not have any major impact on the results. (Fig. 12 shows the UV-based SFR is plotted *versus* the stellar mass in each redshift bin. The UV-based SFR ranges from ~ 0.01 to 25 $M_\odot$ yr^{-1}, with most galaxies having a rate below 5 $M_\odot$ yr^{-1}.

While it is desirable to use the Spitzer 24 μm data in order to account for obscured star formation, only $\sim 24\%$ (~ 878 galaxies) of the 3698 galaxies in our intermediate mass sample have a Spitzer 24 μm detection, although over 86% of the sample is covered by the Spitzer observations down to a limiting flux of $\sim 83 \ \mu$ Jy. The detected galaxies yield a median ratio of (SFR$_{\rm IR}$/SFR$_{\rm UV}$) of ~ 3.6, indicative of a sustantial amount of obscured star formation. Three of the interacting galaxies in the first redshift bin had anomalously high SFR$_{\rm UV+IR}$ (~ 41, 18, and 15 $M_\odot$ yr^{-1}). Two of these turned to have infrared spectra consistent with an AGN and were removed before computing the IR-based SF properties shown in Fig. 13 to Fig. 16.

The average UV-based SFR (based on 3698 galaxies) and UV+IR-based SFR (based on only the 876 galaxies with 24um detections) are plotted in the top 2 panels of Fig. 13 for three groups of intermediate mass galaxies: 'Interacting', 'Non-Interacting E-Sd' and 'Non-Interacting Irr1'. It can be seen that over $z \sim 0.24$–0.80, the average UV-based and UV+IR-based SFR of interacting galaxies (in the phase where they are recognizable as interacting) *are only modestly enhanced*, at best by a factor of a few, compared to the non-interacting galaxies (Fig. 13; see also Robaina et al. in preparation). This modest enhancement is consistent with the recent statistical study of di Matteo et al. (2007), who find from numerical simulations of several hundred galaxy collisions that that the maximum SFR in galaxy mergers is typically only a factor of 2-3 larger than that of corresponding non-interacting galaxies. Their results suggest that the results of some early simulations (e.g., Mihos & Hernquist 1996; Hernquist & Mihos 1995), where mergers converted 50 to 80 per cent of their original gas mass into stars, may not represent the typical situation at $z < 1$.

In order to further test the robustness of our result, we used the stacking procedure de-

scribed in Zheng et al. (2006) to get a more representative measure of the IR-based SFR for the following three groups of intermediate mass galaxies: 'Interacting', 'Non-Interacting E-Sd' and 'Non-Interacting Irr1'. For every group, the individual galaxies were cross-correlated with the Spitzer 24 μm catalog in order to identify detected and undetected objects. Then the PSF-removed 24 μm images for the undetected objects were stacked, and a mean flux was derived from the average/median stacked image. An average 24um luminosity was determined from the individually-detected fluxes and individually-undetected fluxes estimated by stacking. The 3215 intermediate mass galaxies in the Spitzer field were used in this process, giving a more representative 24um luminosity than the mere 878 galaxies with detections. A final uncertainty can be obtained by combining background error and bootstrap error in quadrature. The IR-based SFR was estimated from the 24um luminosity using the procedure described above, and combined with the UV-based SFR to estimate the total SFR. The average UV+IR-stacked SFR is plotted in the bottom panel of Fig. 13: again, only a modest enhancement of a factor of a few is seen in the average SFR of interacting galaxies (in the phase where they are recognizable as interacting), compared to non-interacting galaxies.

4.7. The contribution of interacting galaxies to the cosmic SFR density over the last 7 Gyr

Over the last 8 Gyr since $z \sim 1$, the cosmic SFR density is observed to decline by a factor of 4 to 10 (e.g., Lilly et al. 1996; Ellis et al 1996; Flores et al. 1999; Haarsma et al. 2000; Hopkins 2004; Pérez-González et al. 2005; Le Floc'h et al. 2005). Earlier GEMS studies by Wolf et al. (2005) and Bell et al. (2005) over a 0.6 Gyr interval ($z \sim 0.65$–0.75 or $T_\mathrm{b} \sim 6.2$–6.8 Gyr) strikingly showed that the UV and IR luminosity density over this interval are dominated by non-interacting galaxies. Here, we extend the earlier GEMS studies to cover a six-fold larger time interval of 4 Gyr ($z \sim 0.24$–0.80 or $T_\mathrm{b} \sim 3$–7 Gyr), and set quantitative limits on the contribution of strongly interacting systems to the UV-based and UV+IR-based SFR density. We use the sample S2 of $\sim$3698 intermediate mass ($M \geq 1.0 \times 10^9 \ M_\odot$) galaxies. Our study also complements the IR-based studies by Hammer et al. (2005; l95 galaxies at $z > 0.4$) and Melbourne et al. (2005; ~ 800 galaxies) in terms of sample size and the SFR indicators.

Fig. 14 shows the SFR density for intermediate mass 'Interacting', 'Non-Interacting E-Sd' and 'Non-Interacting Irr1' galaxies over $z \sim 0.24$–0.80. The top panel shows the UV-based SFR density from the full sample. The middle panel show the UV+IR-based SFR density from the 878 galaxies with individual 24um detections. Finally, the bottom panel shows the UV+IR-stacked SFR density determined via the stacking of 3817 galaxies with

Spitzer coverage, as outlined in § 4.6. In all three panels, one finds that *interacting galaxies only account for a small fraction (< 30%) of the cosmic SFR density over z ∼ 0.24–0.80, corresponding to lookback times of 3–7 Gyr (Fig. 13).*

Thus, our results suggest that the behavior of the cosmic SFR density over $z \sim 0.24$–0.80 is predominantly shaped by non-interacting galaxies. This result is a direct consequence of the fact that the interaction interaction fraction f (Table 2; § 4.3), as well as the enhancement in the average SFR from interactions (§ 4.6), are both modest. Our results agree remarkably well with models for the self-regulated growth of supermassive black holes in mergers involving gas-rich galaxies (Hopkins et al. 2005). These models predict that galaxy mergers contribute only $\sim 20\%$ of the SFR density of at $z \sim 1$, and even out out to $z \sim 2$.

It is legitimate to ask whether the results hold despite the uncertainties in identifying strongly interacting galaxies. We first note that based on the tests of § 4.1, we have already included a large fractional error term on f to account for the binomial standard deviation, the dispersion between classifiers, and the effect of moderate bandpass shifting, and surface brightness dimming. Therefore, the results presented here already take into account at least some of these sources of uncertainties.

Another source of uncertainty might be that some of the galaxies, which we have classified as 'Non-Interacting Irr1', under the assumption that their small-scale asymmetries that are likely caused by SF rather than interactions (§ 3.2), may be borderline cases of interacting galaxies. However, it can be seen from Fig. 14, that even if we were to add the SFR density of *all* the 'Non-Interacting Irr1' to that of the interacting galaxies, the sum would still be significantly lower than the contribution of 'Non-Interacting E to Sd' galaxies. Thus, the results would be largely unchanged.

Another test is to repeat the analyses using the CAS merger criterion ($A > 0.35$ and $A > S$) to identify interacting galaxies. The limited recovery rate (40% to 50%) and significant contamination impacting the CAS criterion (§ 3.4) make it more difficult to interpret the SF properties of systems identified as interacting or non-interacting with CAS. Fig. 15 shows that the average SFR of 'CAS-interacting' galaxies is only modestly enhanced compared to 'CAS non-interacting' galaxies, in agreement with the results from § 4.6. Furthermore, Fig. 16 shows that 'CAS-interacting' galaxies contribute only 16% to 33% of the UV SFR density and 22% to 38% of the UV+IR SFR density. While the upper limits of these values are slightly higher than those based on the visual types, it is nonetheless reassuring that 'CAS non-interacting' galaxies' dominate the SFR density.

For intermediate mass ($M \geq 1.0 \times 10^9 \ M_\odot$) galaxies, we find that the cosmic SFR density declines by a factor of ~ 3 from $z \sim 0.80$ to 0.24 (lookback time ~ 7 to 3 Gyr). Since

non-interacting galaxies dominate the cosmic SFR density in every redshift bin, it follows that this decline is largely the result of a shutdown in the SF of relatively non-interacting galaxies. The question of what drives this shutdown will be addressed in detail in a future paper, and is only considered briefly here. One possibility is the depletion of the internal cold gas supply of galaxies by star formation, or the reduction in the accretion rate of gas from cosmological filaments. Future facilities like ALMA will be instrumental in exploring this issue further. Another related possibility is that over time, most of the SFR is shifting to lower stellar masses. This is illustrated in the dependence of the SFR (Fig. 12) and specific SFR (SSFR; Fig. 17) on stellar mass. High mass systems are associated with a lower SSFR (Fig. 17; see also Cowie et al. 1996; Brinchmann et al. 2004; Brinchmann & Ellis 2000; Fontana et al. 2003; Bauer et al. 2005; Zheng et al. 2007; Fig. 1 of Noeske et al. 2007a), consistent with the idea that they have experienced the bulk of their stellar mass growth at earlier epochs ($z > 1$). In staged SF models (Noeske et al. 2007b) the SF history of low mass systems is consistent with exponential SF models associated with an late onset and a long duration.

5. Summary and Conclusions

We have performed a comprehensive observational estimate of the frequency of interacting galaxies over $z \sim 0.24$–0.80 (lookback times of 3–7 Gyr), and explored the impact of interactions on the star formation of galaxies over this interval. Our study is based on *HST* ACS, COMBO-17, and Spitzer 24 μm data from the GEMS survey. We use a large sample of ~ 3600 ($M \geq 1 \times 10^9 \ M_\odot$) galaxies and ~ 790 high mass ($M \geq 2.5 \times 10^{10} \ M_\odot$) galaxies for robust number statistics (§ 2). Two independent methods are used to identify strongly interacting galaxies: a tailored visual classification system complemented with spectrophotometric redshifts and stellar masses (§ 3.2), as well as the CAS merger criterion ($A > 0.35$ and $A > S$), based on CAS asymmetry A and clumpiness S parameters (§ 3.4). This allows one of the most extensive comparisons to date between CAS-based and visual classification results (§ 4.2). We set up this visual classification system so as to target interacting systems whose morphology and other properties suggest they are a recent merger of mass ratio $M1/M2 > 1/10$. While many earlier studies focused on major mergers, we also try to constrain the frequency of minor mergers as well (§ 3.3), since they dominate the merger rates in ΛCDM models. Our results are:

1. We first present results for the high mass ($M \geq 2.5 \times 10^{10} \ M_\odot$) sample, which is complete on both the blue cloud and red sequence. Among ~ 790 high mass galaxies, *the fraction f of visually-classified interacting systems among high mass galaxies remains*

fairly constant over lookback times of 3–7 Gyr, ranging from 9% ± 5% at z ∼ 0.24–0.34, to 8% ± 2% at z ∼ 0.60–0.80, as averaged over every Gyr bin (Table 1; Fig 4). These systems appear to be in merging or post-merger phases, and are candidates for a recent merger of mass ratio $M1/M2 > 1/10$. They are further subdivided into three categories: clear 'major merger', clear 'minor merger', and ambiguous 'major or minor merger' cases. The first two classes are used to set lower limits on the major and minor merger fraction. The lower limit on the major ($M1/M2 > 1/4$) merger fraction, determined in this way, ranges from 1.1% to 3.5% over $z \sim 0.24$–0.80 (Table 1). The corresponding lower limit on the minor ($1/10 \leq M1/M2 < 1/4$) merger fraction ranges from 3.6% to 7.5%. This is the first, albeit approximate, empirical estimate of the frequency of minor mergers over the last 7 Gyr.

For an assumed value of ∼ 0.5 Gyr for the visibility timescale, it follows that *each massive ($M \geq 2.5 \times 10^{10}$ $M_\odot$) galaxy has undergone ∼ 0.7 mergers of mass ratio > 1/10 over the redshift interval z ∼ 0.24–0.80. Of these, we estimate that 1/4 are major mergers, 2/3 are minor mergers, and the rest are ambiguous cases of major or minor mergers.* The corresponding merger rate R is a few $\times 10^{-4}$ galaxies Gyr^{-1} Mpc^{-3}.

2. At intermediate masses ($M \geq 1 \times 10^9$ $M_\odot$) where we are only complete in mass for the blue cloud, we consider f to be meaningful only for the intermediate mass blue cloud sample. *Among ∼ 2840 blue cloud galaxies of mass $M \geq 1.0 \times 10^9$ $M_\odot$, the fraction of interacting galaxies ranges from 7% ± 2% to 15% ± 5% over z ∼ 0.24–0.80 (Table 2).* These systems are candidates for a recent merger of mass ratio $M1/M2 > 1/10$. For an assumed visibility time of ∼ 0.5 Gyr, it follows that over $z \sim 0.24$–0.80 ($T_{\mathrm{back}} \sim 3$–7 Gyr), each intermediate mass blue cloud galaxy has on average undergone ∼ 0.8 mergers of mass ratio > 1/10, of which ∼ 0.05 are major mergers, ∼ 0.15 are minor mergers, and ∼ 0.6 are ambiguous cases of either major or minor mergers. The corresponding merger rate R ranges from 8×10^{-4} to 1×10^{-3} galaxies Gyr^{-1} Mpc^{-3} .

3. The merger fraction based on the CAS merger criterion ($A > 0.35$ and $A > S$) agrees within a factor of two with the visually based interaction fraction for high mass ($M \geq 2.5 \times 10^{10}$ $M_\odot$) galaxies. However, for intermediate mass ($M \geq 1 \times 10^9$ $M_\odot$) galaxies, CAS can overestimate the merger fraction at $z > 0.5$ by a factor ∼ 3. In effect, over $z \sim 0.24$–0.80, ∼ 50% to 70% of the galaxies visually-classified as interacting satisfy the CAS criterion, but the latter also picks up a dominant number of non-interacting dusty, star-forming galaxies (Fig. 7 and Fig. 8). These non-interacting systems make up as much as ∼ 45% to 80% of the systems picked up the CAS criterion. We thus conclude that the traditional CAS merger criterion is ill-suited for use on HST V-band images at $z > 0.5$, where the rest frame wavelength falls below $\lambda < 4000$ Å, particularly in the case of intermediate mass galaxies with significant SF, gas, and dust.

Modified CAS criteria in the near-UV based on morphological k-corrections (Taylor et al. 2007) might alleviate this problem.

4. We compare our empirical merger rate R for high mass ($M \geq 2.5 \times 10^{10}$ $M_\odot$) galaxies to predictions from different ΛCDM-based simulations of galaxy evolution, including the halo occupation distribution (HOD) models of Hopkins et al. (2007); semi-analytic models (SAMs) of Somerville et al. (2008), Bower et al. (2006), and Khochfar & Silk (2006); and smoothed particle hydrodynamics (SPH) cosmological simulations from Maller et al. (2006) with a corrected stellar mass function (see § 4.5). To our knowledge, such extensive comparisons have not been attempted to date, and are long overdue. *We find qualitative agreement between the observations and models, with the (major+minor) merger rate from different models bracketing the observed rate, and showing a factor of five dispersion (Fig. 11).* One can now anticipate that in the near future, improvements in both the observational estimates and model predictions will start to rule out certain merger scenarios and refine our understanding of the merger history of galaxies.

5. We explore the impact of galaxy interactions on the SF properties of galaxies since $z < 0.8$. Among ~ 3600 intermediate mass ($M \geq 1.0 \times 10^9$ $M_\odot$) galaxies, we find that *the average SFR of visibly interacting galaxies is only modestly enhanced compared to non-interacting galaxies over $z \sim 0.24$–0.80 (Fig. 13).* This result is found for SFRs based on UV, UV+IR, as well as UV+stacked-IR data. This modest enhancement is consistent with the empirical results of Robaina et al. (in preparation), and the recent statistical study of di Matteo et al. (2007) based on numerical simulations of several hundreds of galaxy collisions.

6. Among these ~ 3600 intermediate mass ($M \geq 1.0 \times 10^9$ $M_\odot$) galaxies, our results of a modest interaction fraction f and a modest enhancement in SFR from interactions culminate in our finding that *visibly interacting systems only account for a small fraction ($< 30\%$) of the cosmic SFR density over lookback times of ~ 3–7 Gyr ($z \sim 0.24$–0.80; Fig. 14).* Our result is consistent with that of Wolf et al. (2005) over a smaller lookback time interval of ~ 6.2–6.8 Gyr. In effect, our result suggests that *the behavior of the cosmic SFR density over the last 7 Gyr is predominantly shaped by non-interacting galaxies, rather than strongly interacting galaxies.* We suggest that our observed decline in the cosmic SFR density by a factor of ~ 3 since $z \sim 0.80$ is largely the result of a shutdown in the SF of relatively non-interacting galaxies. This shutdown may be driven by the depletion of the internal cold gas supply of galaxies, the reduction in the accretion rate of gas from cosmological filaments, and the transition of SF activity to lower mass systems.

REFERENCES

Alexander, D. M., et al. 2003, AJ, 126, 539

Barazza, F. D., Jogee, S., & Marinova, I. 2007, IAU Symposium, 235, 76

Barden, M., et al. 2005, ApJ, 635, 959

Barden, M., Jahnke, K., Haumlußler, B. 2008, ApJS, 175, 105

Barnes, J. E., & Hernquist, L. E. 1991, ApJL, 370, L65

Barnes, J. E., & Hernquist, L. 1996, ApJ, 471, 115

Barton Gillespie, E., Geller, M. J., & Kenyon, S. J. 2003, ApJ, 582, 668

Bauer, A. E., Drory, N., Hill, G. J., & Feulner, G. 2005, ApJL, 621, L89

Bell, E. F., et al. 2004, ApJL, 600, L11

Bell, E. F., et al. 2005, ApJ, 625, 23

Bell, E. F., Phleps, S., Somerville, R. S., Wolf, C., Borch, A., & Meisenheimer, K. 2006, ApJ, 652, 270

Bell, E. F., Zheng, X. Z., Papovich, C., Borch, A., Wolf, C., & Meisenheimer, K. 2007, ApJ, 663, 834

Benson, A. J., Lacey, C. G., Frenk, C. S., Baugh, C. M., & Cole, S. 2004, MNRAS, 351, 1215

Benson, A. J., Kamionkowski, M., & Hassani, S. H. 2005, MNRAS, 357, 847

Bershady, M. A., Jangren, A., & Conselice, C. J. 2000, AJ, 119, 2645

Binney, J., & Merrifield, M. 1998, Galactic astronomy / James Binney and Michael Merrifield. Princeton, NJ : Princeton University Press, 1998. (Princeton series in astrophysics) QB857 .B522 1998 ($35.00),

Binney, J., & Tremaine, S. 1987, Princeton, NJ, Princeton University Press, 1987, 747 p.,

Borch, A., et al. 2006, A&A, 453, 869

Bower, R. G., Benson, A. J., Malbon, R., Helly, J. C., Frenk, C. S., Baugh, C. M., Cole, S., & Lacey, C. G. 2006, MNRAS, 370, 645

Boylan-Kolchin, M., Ma, C.-P., & Quataert, E. 2008, MNRAS, 383, 93

Brand, K., et al. 2006, ApJ, 644, 143

Brand, K., et al. 2006, ApJ, 641, 140

Brinchmann, J., Charlot, S., White, S. D. M., Tremonti, C., Kauffmann, G., Heckman, T., & Brinkmann, J. 2004, MNRAS, 351, 1151

Brinchmann, J., & Ellis, R. S. 2000, ApJL, 536, L77

Cassata, P., et al. 2005, MNRAS, 357, 903

Caldwell, J. A. R., et al. 2008, ApJS, 174, 136

Chabrier, G. 2003, PASP, 115, 763

Cole, S., Lacey, C. G., Baugh, C. M., & Frenk, C. S. 2000, MNRAS, 319, 168

Conselice, C. J., Bershady, M. A., & Jangren, A. 2000, ApJ, 529, 886

Conselice, C. J. 2003, ApJS, 147, 1

Conselice, C. J., Bershady, M. A., Dickinson, M., & Papovich, C. 2003, AJ, 126, 1183

Conselice, C. J., Blackburne, J. A., & Papovich, C. 2005, ApJ, 620, 564

Conselice, C. J. 2006, ApJ, 638, 686

Conselice, C. J., Rajgor, S., & Myers, R. 2008, MNRAS, 386, 909

Cowie, L. L., Songaila, A., Hu, E. M., & Cohen, J. G. 1996, AJ, 112, 839

Cox, T. J., Jonsson, P., Primack, J. R., & Somerville, R. S. 2006, MNRAS, 373, 1013

Cox, T. J., Dutta, S. N., Di Matteo, T., Hernquist, L., Hopkins, P. F., Robertson, B., & Springel, V. 2006, ApJ, 650, 791

Cox, T. J., Di Matteo, T., Hernquist, L., Hopkins, P. F., Robertson, B., & Springel, V. 2006, ApJ, 643, 692

Croton, D. J., et al. 2006, MNRAS, 367, 864

Croton, D. J., et al. 2006, MNRAS, 365, 11

De Propris, R., Conselice, C. J., Liske, J., Driver, S. P., Patton, D. R., Graham, A. W., & Allen, P. D. 2007, ApJ, 666, 212

Devriendt, J. E. G., Guiderdoni, B., & Sadat, R. 1999, A&A, 350, 381

D'Onghia, E., & Burkert, A. 2004, ApJL, 612, L13

D'Onghia, E., Mapelli, M., Moore, B. 2008, MNRAS, submitted (arXiv:0803.0545)

di Matteo, P., Combes, F., Melchior, A.-L., & Semelin, B. 2007, A&A, 468, 6

Ellis, R. S., Colless, M., Broadhurst, T., Heyl, J., & Glazebrook, K. 1996, MNRAS, 280, 235

Fakhouri, O, Ma, C.-P., 2008, MNRAS, 386, 577

Flores, H., et al. 1999, ApJ, 517, 148

Fontana, A., et al. 2003, ApJL, 594, L9

Fontana, A., Poli, F., Menci, N., Nonino, M., Giallongo, E., Cristiani, S., & D'Odorico, S. 2003, ApJ, 587, 544

Franceschini, A., et al. 2005, AJ, 129, 2074

Gordon, K. D., et al. 2005, PASP, 117, 503

Gottloeber, S., Klypin, A., Kravtsov, A. V. 2001, ApJ, 546, 223

Governato, F., et al. 2004, ApJ, 607, 688

Haarsma, D. B., Partridge, R. B., Windhorst, R. A., & Richards, E. A. 2000, ApJ, 544, 641

Hammer, F., Flores, H., Elbaz, D., Zheng, X. Z., Liang, Y. C., & Cesarsky, C. 2005, A&A, 430, 115

Hernquist, L. 1989, Nature, 340, 687

Hernquist, L., & Mihos, J. C. 1995, ApJ, 448, 41

Hopkins, P. F., Somerville, R. S., Hernquist, L., Cox, T. J., Robertson, B., & Li, Y. 2006, ApJ, 652, 864

Hopkins, A. M. 2004, ApJ, 615, 209

Hopkins et al. 2008, ApJ, submitted (arXiv:0706.1243)

Jogee, S., Kenney, J. D. P., & Smith, B. J. 1998, ApJL, 494, L185

Jogee, S., Kenney, J. D. P., & Smith, B. J. 1999, ApJ, 526, 665

Jogee, S., 1999, Ph.D. thesis, Yale University

Jogee, S., 2006, Lecture Notes in Physics, Vol. 693, "AGN Physics on All Scales", Eds. D. Alloin, R. Johnson, & P. Lira (Springer: Berlin Heidelberg New York), Vol 93, Chapter 6, p 143 (astro-ph/0408383).

Jogee, S. et al. 2008, in Formation and Evolution of Galaxy Disks, ed. J. G. Funes, S. J., & E. M. Corsini (San Francisco:ASP), in press (arXiv:0802.3901)

Joseph, R. D., & Wright, G. S. 1985, MNRAS, 214, 87

Kartaltepe, J. S., et al. 2007, ApJS, 172, 320

Kauffmann, G., White, S. D. M., & Guiderdoni, B. 1993, MNRAS, 264, 201

Kautsch, S. J., Grebel, E. K., Barazza, F. D., & Gallagher, J. S., III 2006, A&A, 451, 1171

Kennicutt, R. C., Roettiger, K. A., Keel, W. C., Vanderhulst, J. M., & Hummel, E. 1987, NASA Conference Publication, 2466, 401

Kennicutt, R. C.,Jr., Roettiger, K. A., Keel, W. C., van der Hulst, J. M., & Hummel, E. 1987, AJ, 93, 1011

Khochfar, S., & Burkert, A. 2001, ApJ, 561, 517

Khochfar, S., & Burkert, A. 2005, MNRAS, 359, 1379

Khochfar, S., & Silk, J. 2006, MNRAS, 370, 902

Koopmann, R. A., & Kenney, J. D. P. 1998, ApJL, 497, L75

Kroupa, P. 2001, MNRAS, 322, 231

Kroupa, P., Tout, C. A., & Gilmore, G. 1993, MNRAS, 262, 545

Lacey, C., Cole, S. 1993, MNRAS, 262, 627

Larson, R. B., & Tinsley, B. M. 1978, ApJ, 219, 46

Le Floc'h, E., et al. 2005, ApJ, 632, 169

Le Fèvre, O., et al. 2000, MNRAS, 311, 565

Lehmer, B. D., et al. 2005, ApJS, 161, 21

Lilly, S. J., Le Fevre, O., Hammer, F., & Crampton, D. 1996, ApJL, 460, L1

Lin, L., et al. 2004, ApJL, 617, L9

Lotz, J. M., Primack, J., & Madau, P. 2004, AJ, 128, 163

Lotz, J. M., et al. 2008, ApJ, 672, 177

Madau, P., Ferguson, H. C., Dickinson, M. E., Giavalisco, M., Steidel, C. C., & Fruchter, A. 1996, MNRAS, 283, 1388

Madau, P., della Valle, M., & Panagia, N. 1998, MNRAS, 297, L17

Maller, A. H., Katz, N., Kereš, D., Davé, R., & Weinberg, D. H. 2006, ApJ, 647, 763

Melbourne, J., Koo, D. C., & Le Floc'h, E. 2005, ApJL, 632, L65

Mihos, J. C., Walker, I. R., Hernquist, L., Mendes de Oliveira, C., & Bolte, M. 1995, ApJL, 447, L87

Mihos, J. C., & Hernquist, L. 1994, ApJ, 437, 611

Mihos, J. C., & Hernquist, L. 1996, ApJ, 464, 641

Miller, S. H., et al. 2008, ArXiv e-prints, 802, arXiv:0802.3917

Murali, C., Katz, N., Hernquist, L., Weinberg, D. H., & Davé, R. 2002, ApJ, 571, 1

Naab, T., & Burkert, A. 2001, ApJL, 555, L91

Navarro, J. F., & Benz, W. 1991, ApJ, 380, 320

Navarro, J. F., & Steinmetz, M. 2000, ApJ, 538, 477

Navarro, J. F., & Steinmetz, M. 2000, ApJ, 528, 607

Negroponte, J., & White, S. D. M. 1983, MNRAS, 205, 1009

Neistein, E., Dekel, A., eprint arXiv:0802.0198

Noeske, K. G., et al. 2007a, ApJL, 660, 43

Noeske, K. G., et al. 2007b, ApJL, 660, L47

Papovich, C., & Bell, E. F. 2002, ApJL, 579, L1

Papovich, C., et al. 2004, ApJS, 154, 70

Patton, D. R., Carlberg, R. G., Marzke, R. O., Pritchet, C. J., da Costa, L. N., & Pellegrini, P. S. 2000, ApJ, 536, 153

Patton, D. R., et al. 2002, ApJ, 565, 208

Pérez-González, P. G., et al. 2005, ApJ, 630, 8

Rieke, G. H., et al. 2004, ApJS, 154, 25

Rix, H.-W., et al. 2004, ApJS, 152, 163

Robertson, B., Yoshida, N., Springel, V., & Hernquist, L. 2004, ApJ, 606, 32

Smith, B. J. 1994, AJ, 107, 1695

Somerville, R. S., & Primack, J. R. 1999, MNRAS, 310, 1087

Somerville, R. S. & Kolatt, T. S. 1999, MNRAS, 305, 1

Somerville, R. S., et al. 2008, ApJ, 672, 776

Springel, V., Di Matteo, T., & Hernquist, L. 2005, MNRAS, 361, 776

Springel, V., Di Matteo, T., & Hernquist, L. 2005, MNRAS, 361, 776 ’

Struck, C. 1997, ApJS, 113,269

Taylor-Mager, V. A., Conselice, C. J., Windhorst, R. A., & Jansen, R. A. 2007, ApJ, 659, 162

van den Bosch, F. C. et al., 2007, MNRAS, 376, 841

Weinzirl, T., Jogee, S., Khochfar, S., Burkert, A., & Kormendy, J. 2008, ApJ, submitted.

Wolf, C., et al. 2004, A&A, 421, 913

Wolf, C., et al. 2005, ApJ, 630, 771

Zheng et al. 2006, ApJ, 640, 784

Zheng, X. Z., Bell, E. F., Papovich, C., Wolf, C., Meisenheimer, K., Rix, H.-W., Rieke, G. H., & Somerville, R. 2007, ApJL, 661, L41
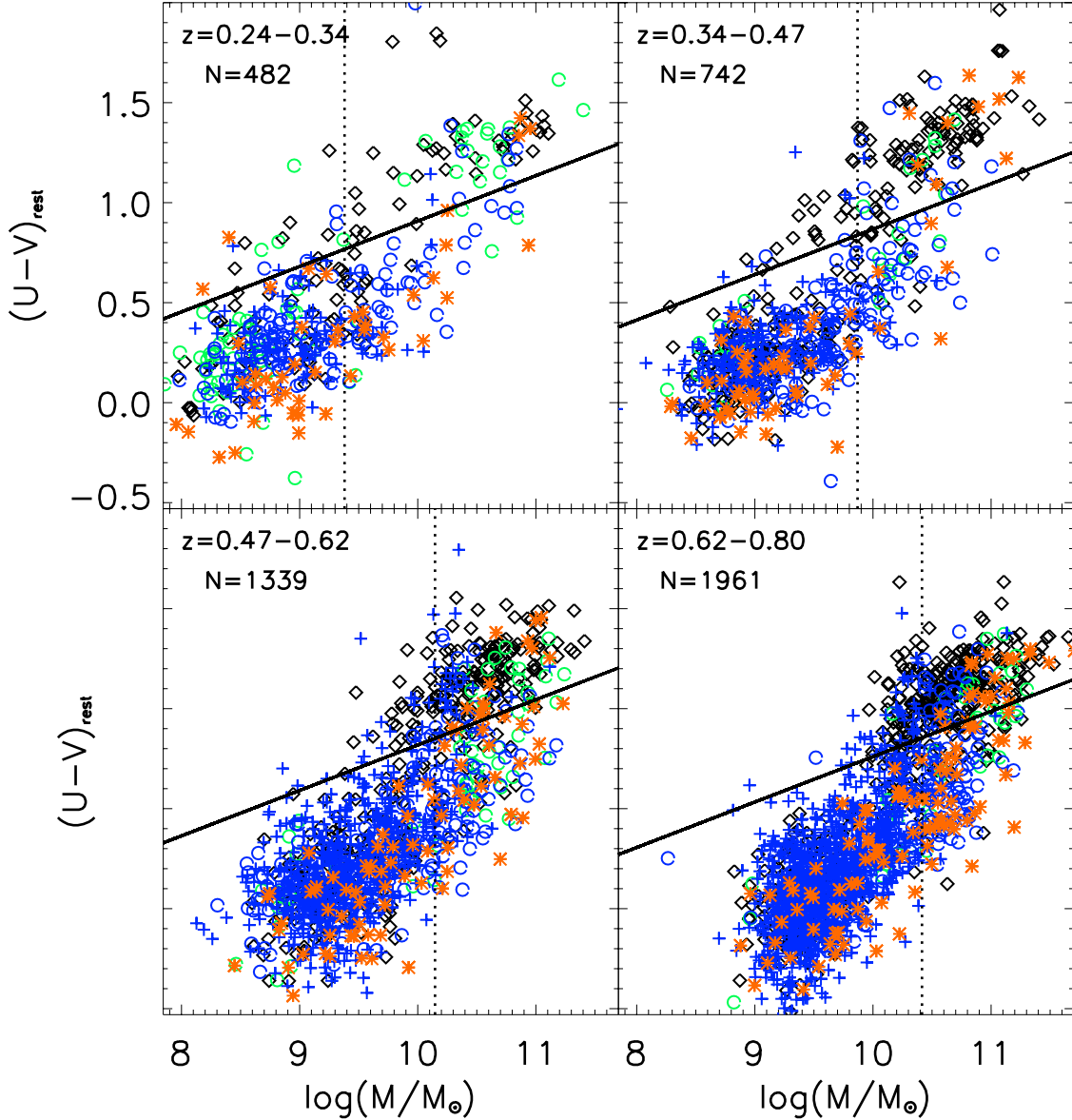
Fig. 1.— The rest-frame $U - V$ color is plotted *versus* the stellar mass in four redshift bins, which span 1 Gyr each, and cumulatively cover the interval $z \sim 0.24$–0.80 ($T_{back} \sim 3$–7 Gyr). N denotes the number of galaxies in each bin. The diagonal line marks the separation of the red sequence galaxies and the blue cloud galaxies at the average redshift z_{ave} of the bin. The vertical lines marks the mass completeness limit (Borch et al. (2006)) for the red sequence galaxies. The blue cloud galaxies are complete well below this mass. Galaxies are coded according to their visual type (VT) in the F606W band: 'Interacting' (orange stars), 'Non-Interacting E-Sd' (E+S0=black diamonds, Sa=green circles, Sb-Sc=blue circles, Sd=blue crosses), and 'Non-Interacting Irr1' (blue crosses) galaxies.
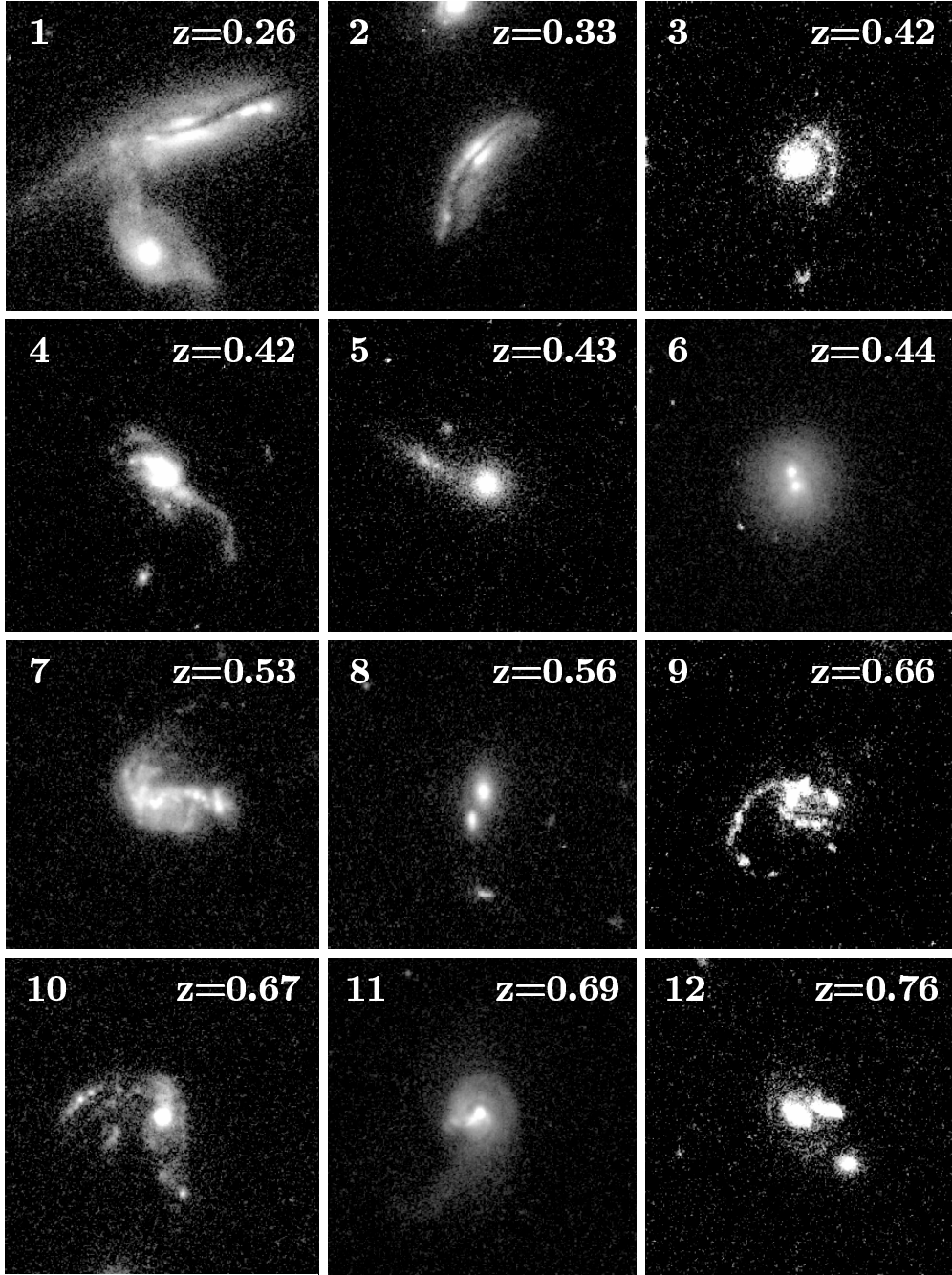
Fig. 2.— This montage show examples of galaxies classified as interacting ('Int') galaxies. These are candidates for a recent/ongoing interaction of mass ratio $M1/M2 > 1/10$. Systems classified as 'Int-1' show morphological distortions, such as multiple nuclei (e.g., 6, 8) or components (e.g., 12) connected by a bridge or common envelope, warped disks (e.g., 2), tidal tails (e.g., 3, 4, 5, 9, 11), strongly asymmetric features, or accreting companions (e.g., 1, 12). The lower galaxy in case 1 is an example of an 'Int-2' system or contact pair: it is *fairly symmetric*, but it has a companion, which satisfies four criteria: it has the same COMBO-17 spectrophotometric redshift within the accuracy $\delta_z/(1 + z) \sim 0.02$, has a stellar mass ratio satisfying $M1/M2 > 1/10$, and shares a common envelope/bridge of light.
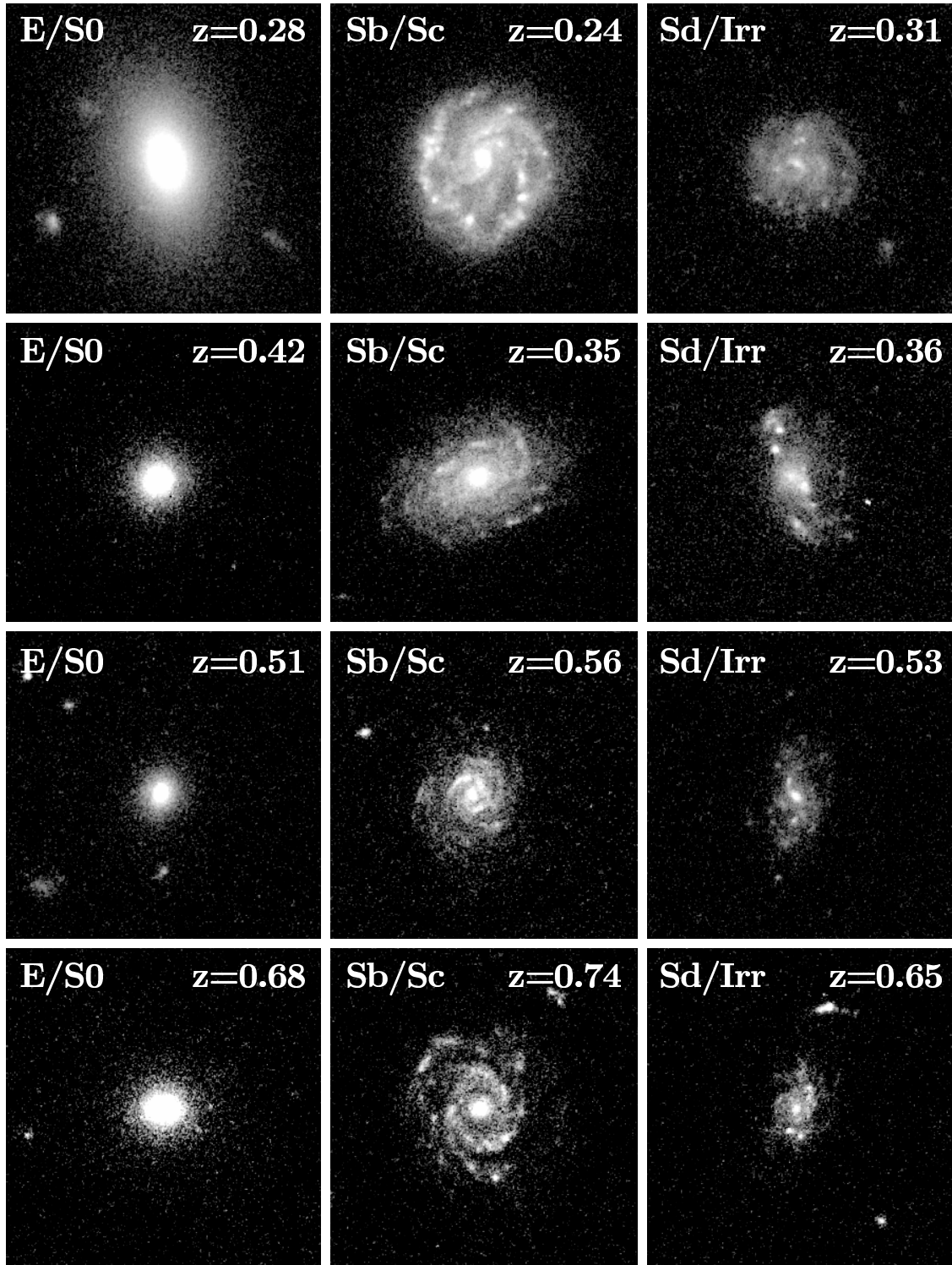
Fig. 3.— This montage shows examples of galaxies classified as 'Non-Interacting E-Sd' and ' Non-Interacting Irr1' galaxies. They are subdivided as E/S0, Sb/Sc and Sd/Irr1. The four rows show candidates from the four redshift bins in Figure 1.
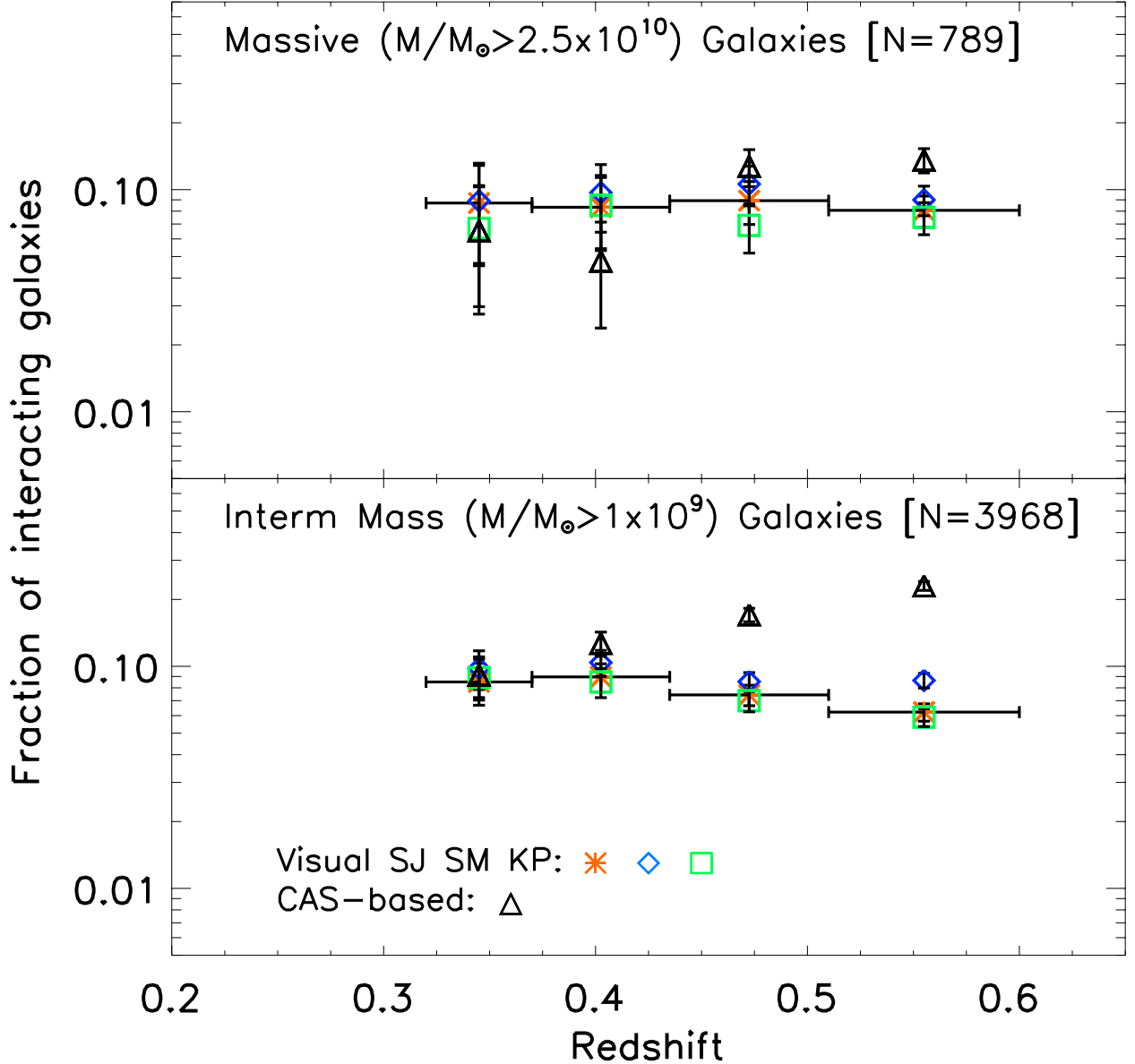
Fig. 4.— This figure compares the fraction (f) of strongly interacting galaxies,, based on visual classification by 3 classifiers (SJ, SM, KP), to the interaction fraction (f_{CAS}) that would be obtained using the CAS criterion ($A > 0.35$ and $A > S$). The results are shown for both high mass ($M \geq 2.5 \times 10^{10}$ $M_\odot$; top panel) and intermediate mass ($M \geq 1 \times 10^9$ $M_\odot$; bottom panel) sample. The plotted error bar for f, at this stage, only includes the binomial term $[f(1-f)/N]^{1/2}$, for each bin of size N. The same trend is seen for all 3 classifiers and the maximum spread δ_f/f in the 4 bins is $\sim 26\%$. f_{CAS} agrees within a factor of two with the visually based f interaction fraction for high mass galaxies. However, for intermediate mass galaxies, CAS can overestimate the interaction fraction at $z > 0.5$ by a factor ~ 3, as it picks up a significant number of non-interacting dusty, star-forming galaxies (see § 4.2).
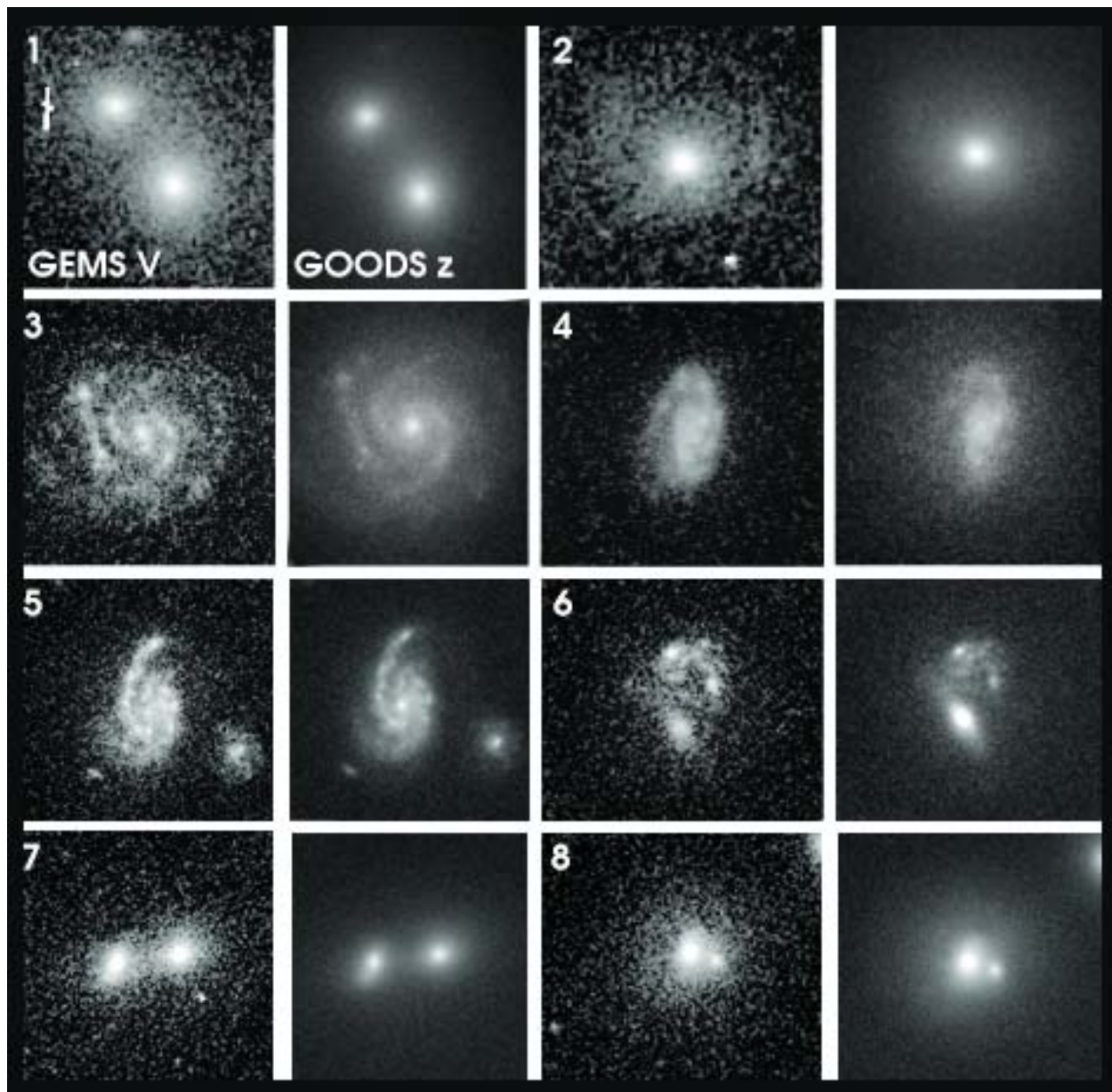
Fig. 5.— This montage illustrates a test for bandpass shift and surface brightness dimming. It compares the bluer shallower GEMS F606W images (V band; pivot $\lambda \sim 5915$ Å) and deeper redder GOODS F850LP (z band; pivot $\lambda \sim 9103$ Å) images of typical interacting and non-interacting galaxies in the last redshift bin ($z \sim 0.60$ to 0.80), where bandpass shift and surface brightness dimming are expected to be most severe. In this redshift bin, the rest-frame wavelength traced by the GEMS images shift from optical to violet/near-UV (3700 Å to 3290 Å). However, while the GOODS images have higher S/N, and trace redder older stars, they do not reveal dramatically different morphologies from from those in the GEMS F606W images. A statistical analysis is shown in Table 3.
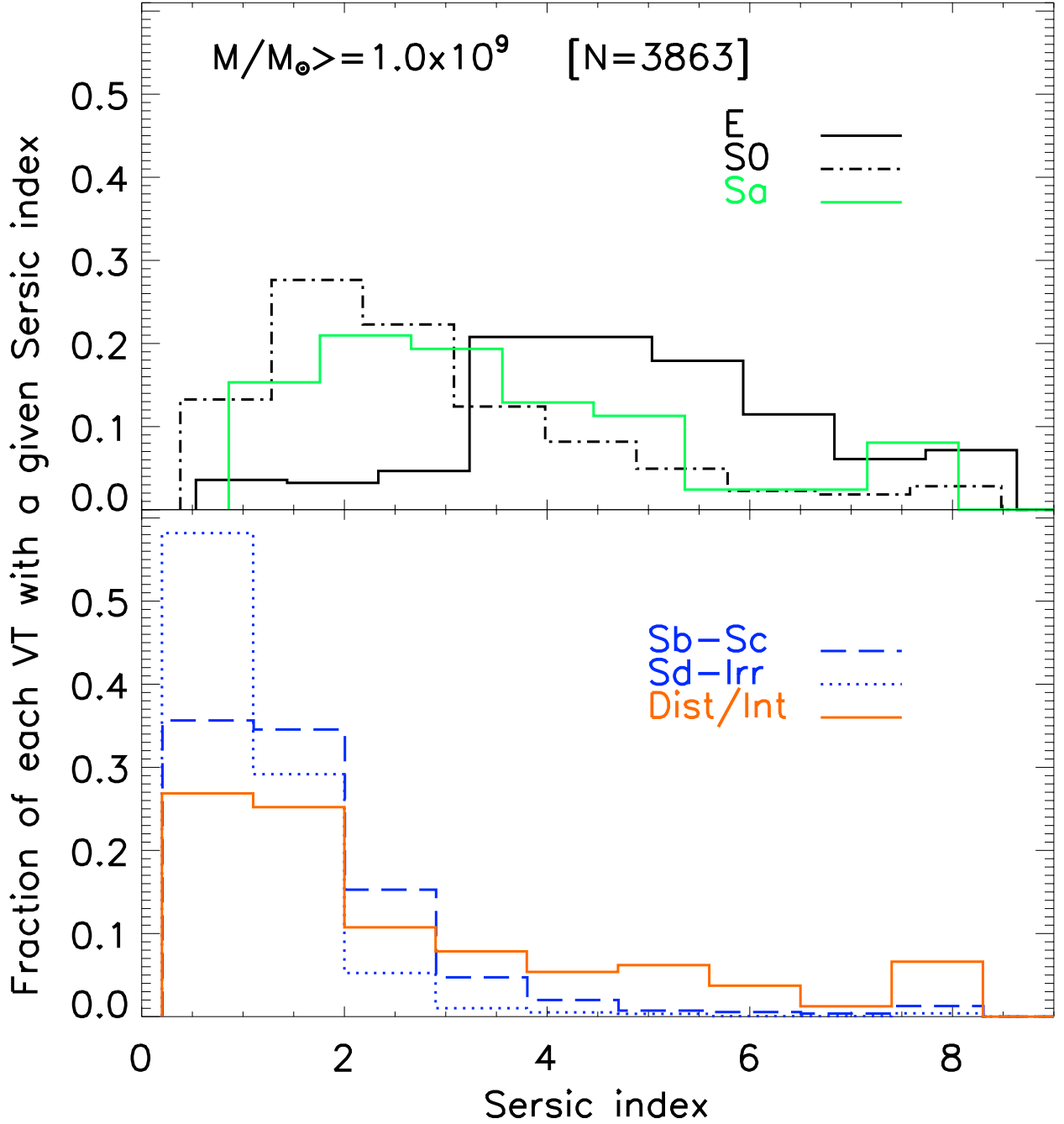
Fig. 6.— For intermediate mass ($M \geq 1 \times 10^9 \, M_\odot$) galaxies, the distribution of Sérsic indices n from single-component Sérsic fits is plotted for interacting , 'non-Interacting E-Sd' and 'non-Interacting Irr1' galaxies. The latter classes are further subdivided as E/S0, Sb/Sc and Sd/Irr1. The majority of systems visually classified as Sb-Sc and Sd-Irr have $n < 2.5$, as expected for disk-dominated systems. Most of the systems visually typed as E have $n > 3$ and their distribution peaks at $n \sim 4$, corresponding to a de Vaucouleurs profile. S0 and Sa systems have intermediate n values.
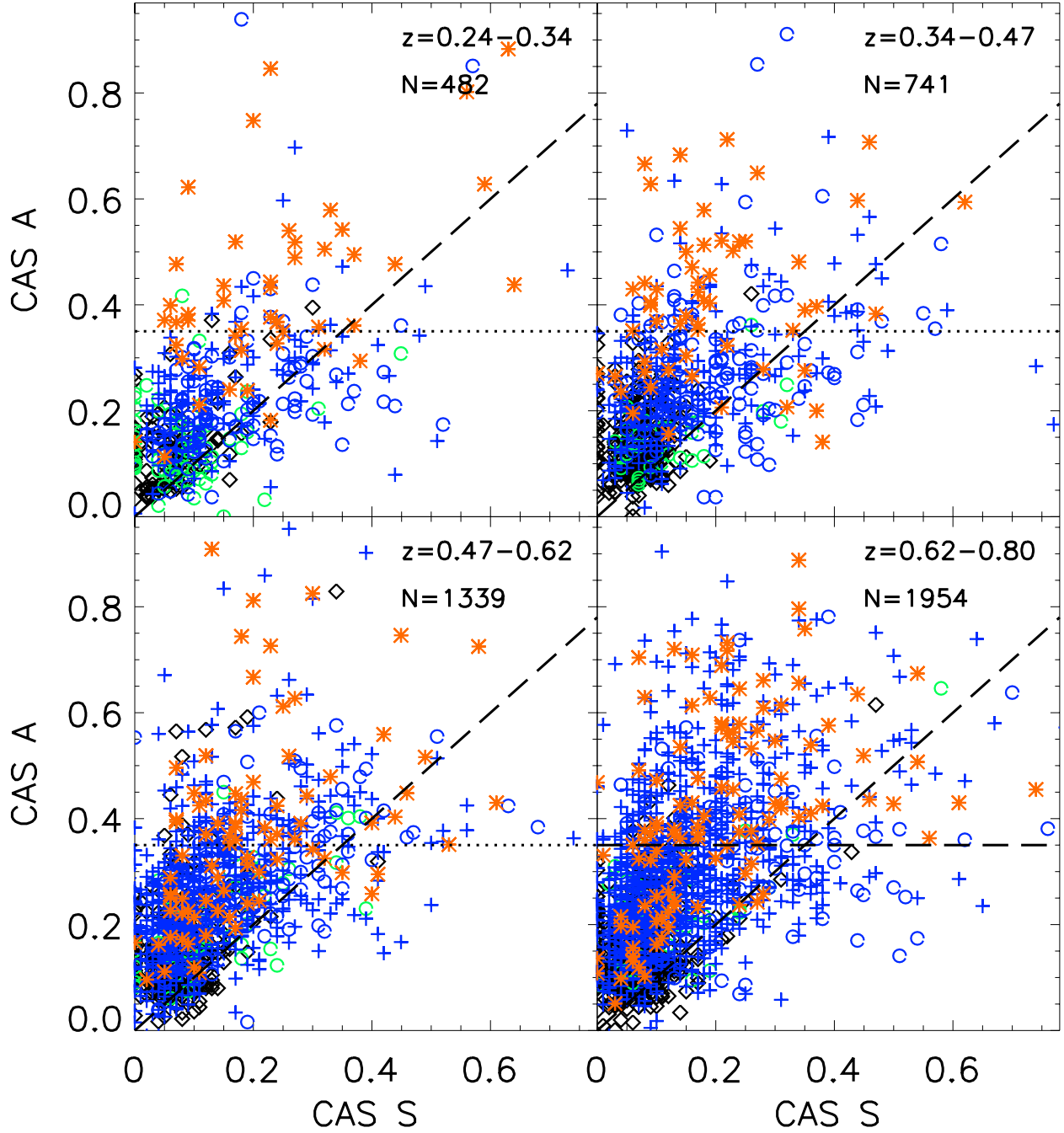
Fig. 7.— The CAS asymmetry A and clumpiness S parameters are plotted for galaxies in the four redshift bins of Fig. 1, using the same color coding. Galaxies satisfying the CAS criterion ($A > 0.35$ and $A > S$) lie in the upper left hand corner, bracketed by the $A = S$ diagonal line and the $A = 0.35$ horizontal line. The CAS criterion captures a fair fraction of the strongly interacting galaxies, but it also picks up "contaminants" in the form of non-interacting galaxies. This is further illustrated in Fig. 8.
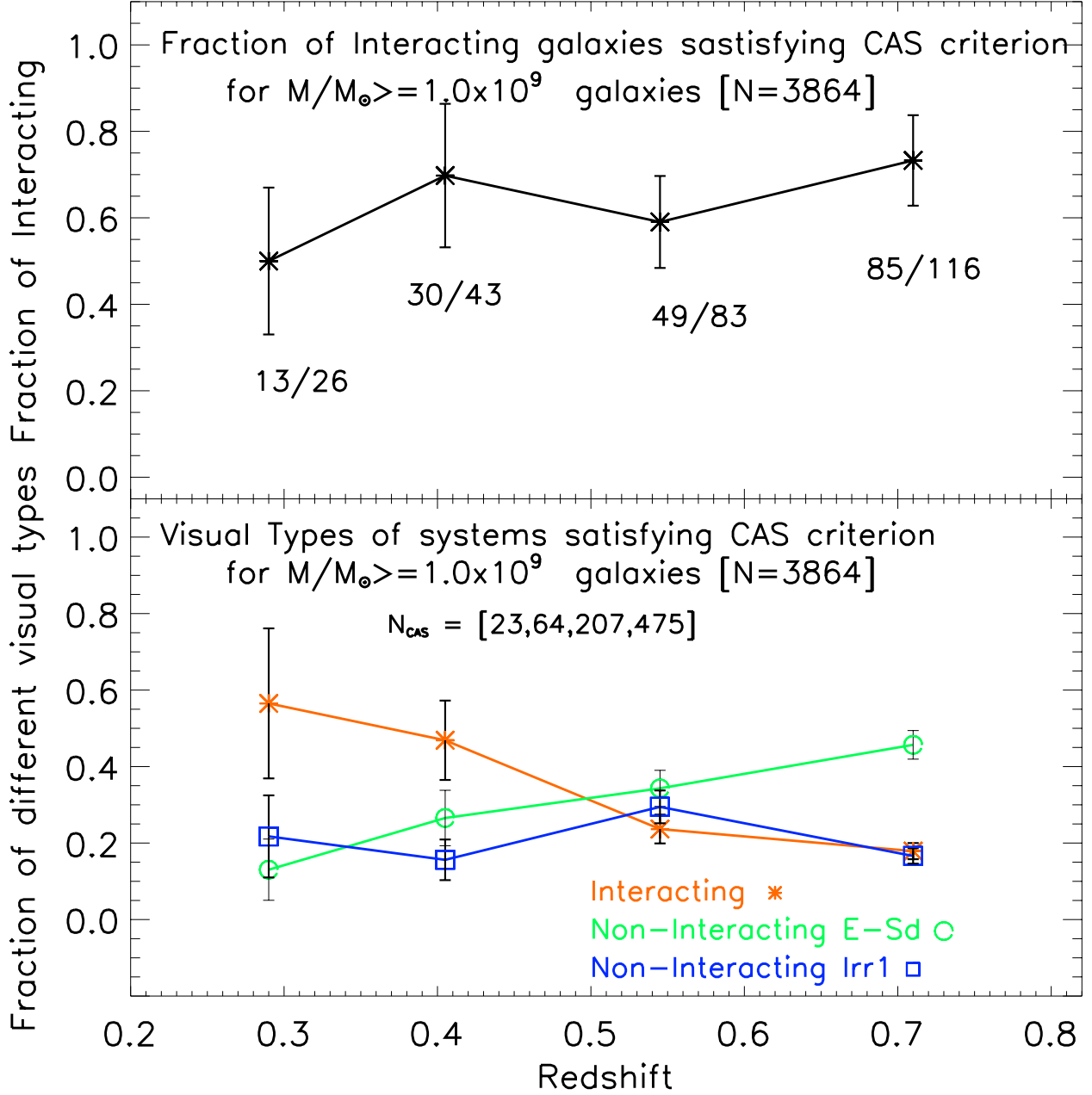
Fig. 8.— This figure includes only intermediate mass ($M \geq 1.0 \times 10^9 \ M_\odot$) galaxies. The top panel shows that the fraction of visually-classified interacting galaxies that satisfy the CAS criterion is $\sim$ 50% to 70% across the four redshift bins. The bottom panel shows the contamination level of the CAS system by non-interacting galaxies. $N_{\rm CAS}$ represents the total number of galaxies satisfying the CAS criterion in the four redshift bins. The distribution of visual types among these systems is plotted. The vast majority (44% to 80%) of sytems picked up by CAS at $z > 0.5$ are non-interacting systems [E-Sd and Irr].
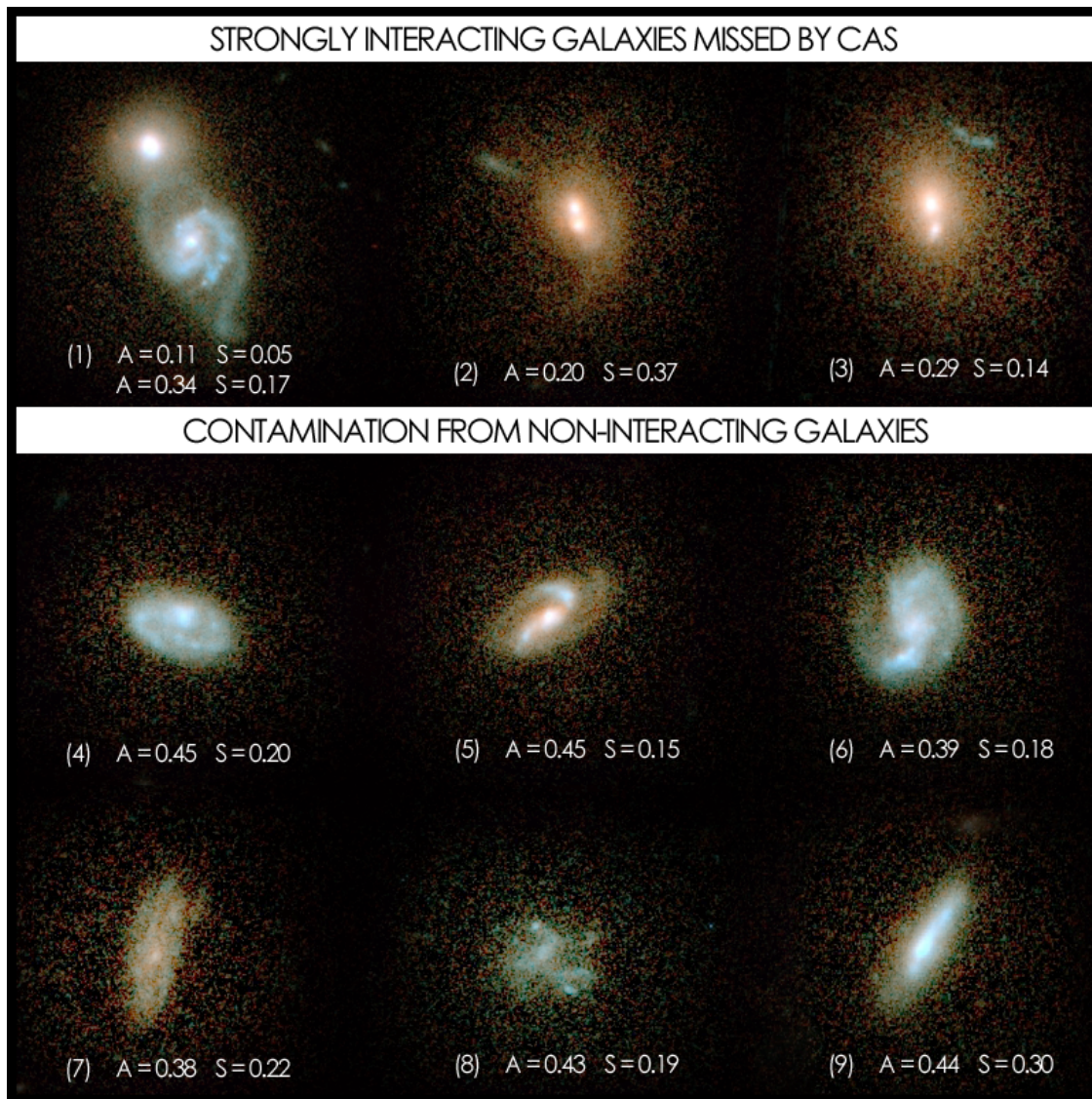
Fig. 9.— The montage shows typical systems where the CAS criterion ($A > 0.35$ and $A > S$) fails. Cases 1-3 are systems, which are visually classified as strongly interacting, but are missed by the CAS criterion. They include galaxies with tidal debris (Case 3), close double nuclei (case 2), and galaxies at the same redshift connected via tidal features (case 1). Conversely, cases 4-9 are systems, which are visually classified as non-interacting galaxies, but are picked by the CAS criterion. They include non-interacting, actively star-forming systems with small-scale asymmetries in the optical blue light (cases 4 and 6); systems where A is high due to the absence of a clear center (case 8) or due to the center being blocked by dust (case 4, 9); edge-on systems and compact systems, where the light profile is steep such that small centering inaccuracies lead to large A (case 9).
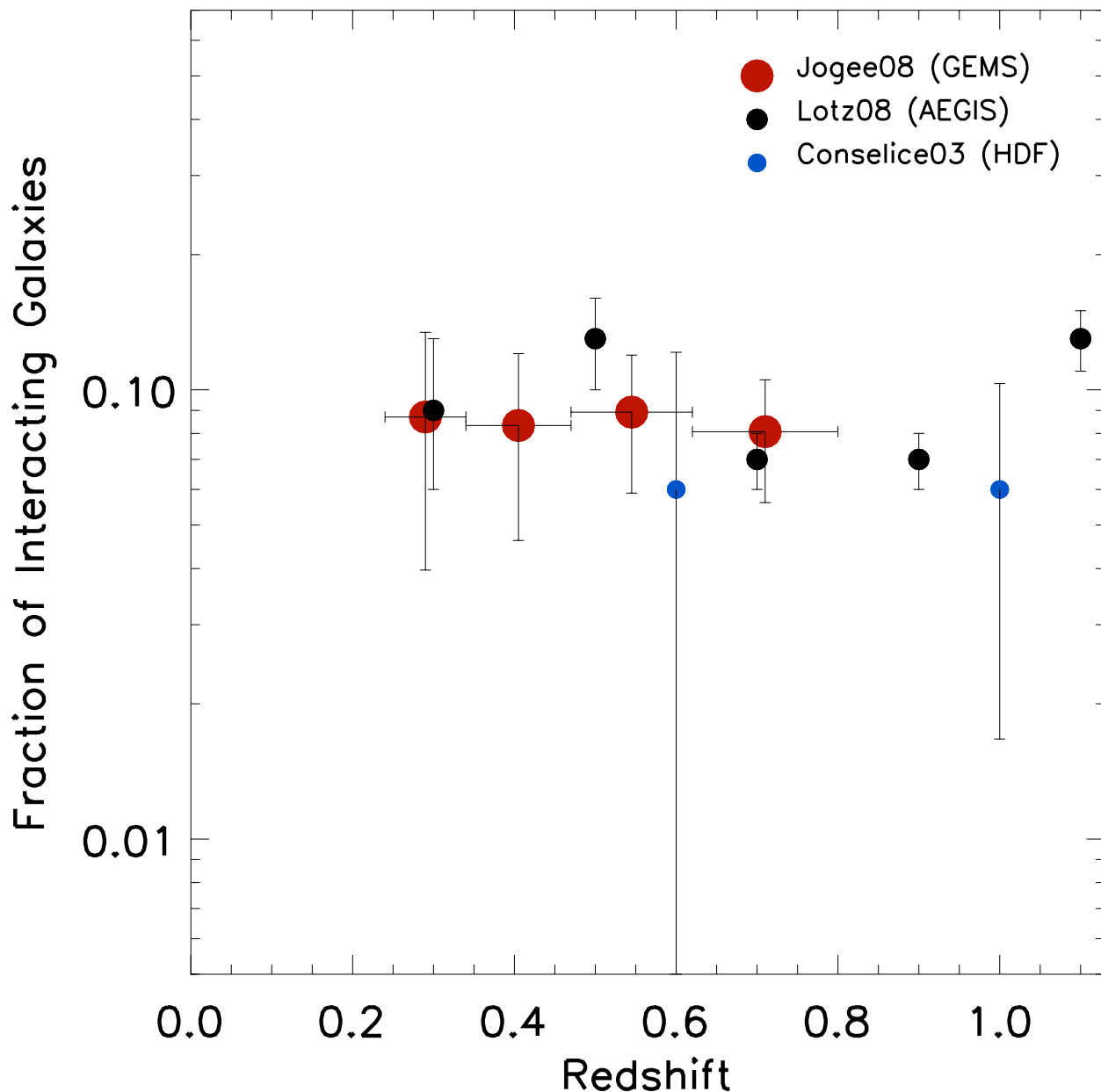
Fig. 10.— The observed fraction f of interacting galaxies in the high mass ($M \geq 2.5 \times 10^{10}$ $M_{\odot}$) sample is compared to other studies, noting the caveats outlined in § 4.4. Shown here is the fraction of morphologically disturbed systems based on Gini-M20 parameters among $M_{B} < $ -20.5 and $L_{B} > 0.4$ L_{*} galaxies in the Extended Groth Strip (Lotz et al. (2008). The CAS-based results from Conselice (2003) are derived from a small sample in the Hubble Deep Field.
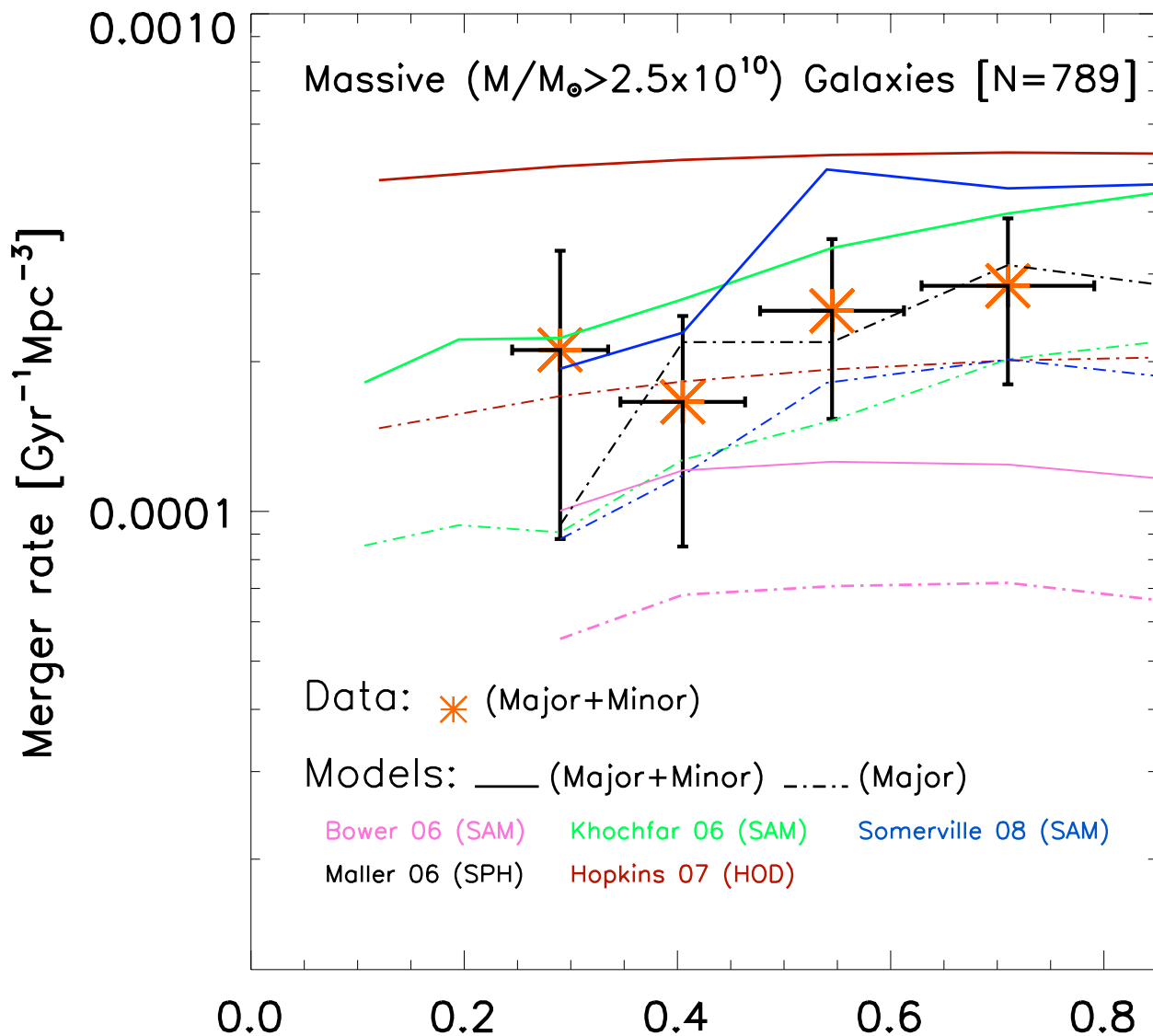
Fig. 11.— The empirical rate R (orange stars) of mergers with mass ratio $M1/M2 > 1/10$. among high mass galaxies is compared to the rate of (major+minor) mergers (solid lines; stellar mass ratio $M1/M2 > 1/10$) predicted by different ΛCDM-based simulations of galaxy evolution, including the halo occupation distribution (HOD) models of Hopkins et al. (2007); semi-analytic models (SAMs) of Somerville et al. (2008), Bower et al. (2006), and Khochfar & Silk (2006); and smoothed particle hydrodynamics (SPH) cosmological simulations from Maller et al. (2006) (see § 4.5).
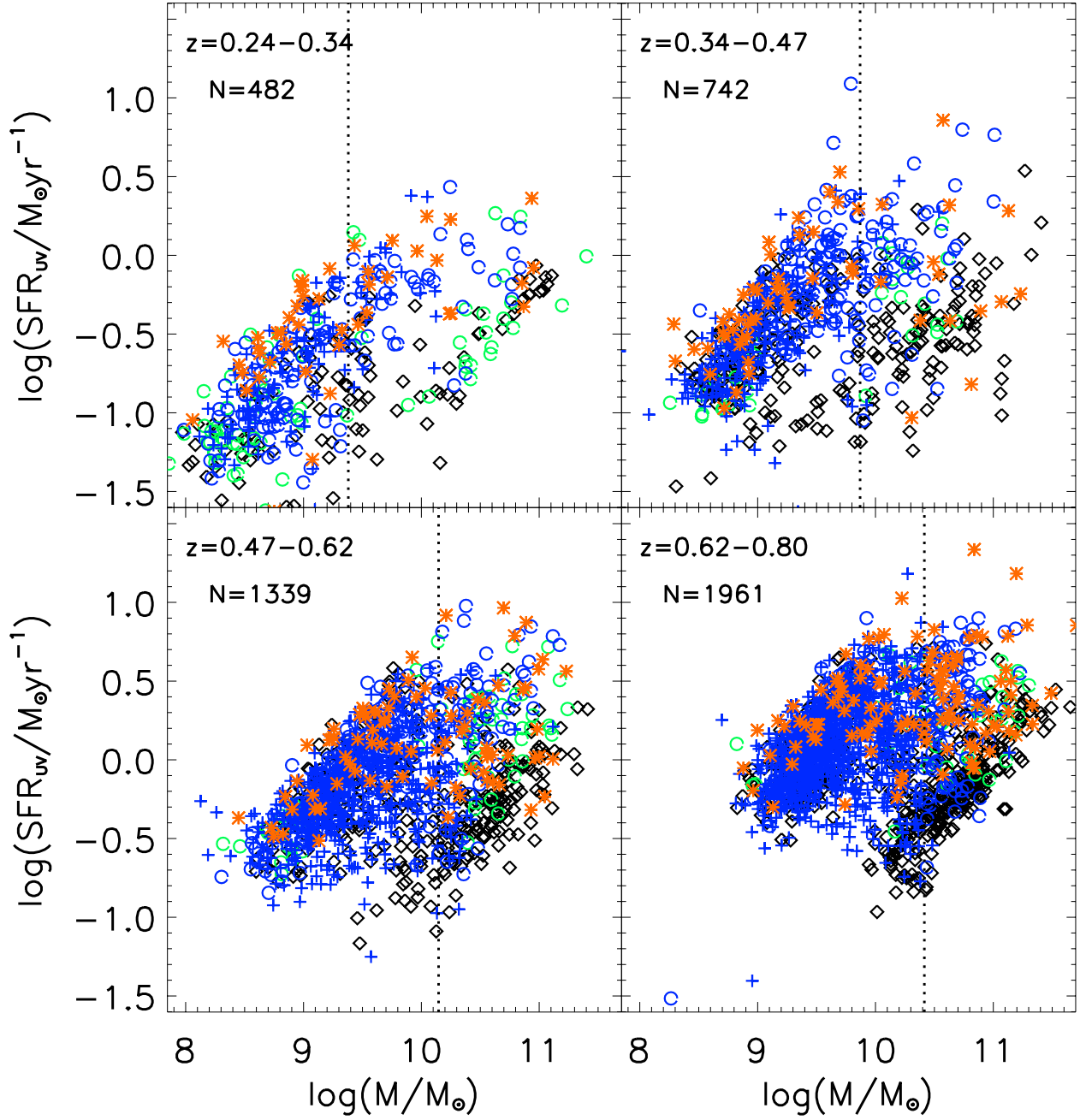
Fig. 12.— The UV-based star formation rate is plotted *versus* the stellar mass in four redshift bins, which span 1 Gyr each, and cumulatively cover the interval $z \sim 0.24$–0.80 ($T_{\mathrm{back}} \sim 3$–7 Gyr). N denotes the number of galaxies plotted in each bin. Galaxies are coded as in Fig. 1, with strongly interacting systems denoted by orange stars. The average SFR and total SFR density in both the UV and the IR, are further illustrated in Fig. 13 and Fig. 14.
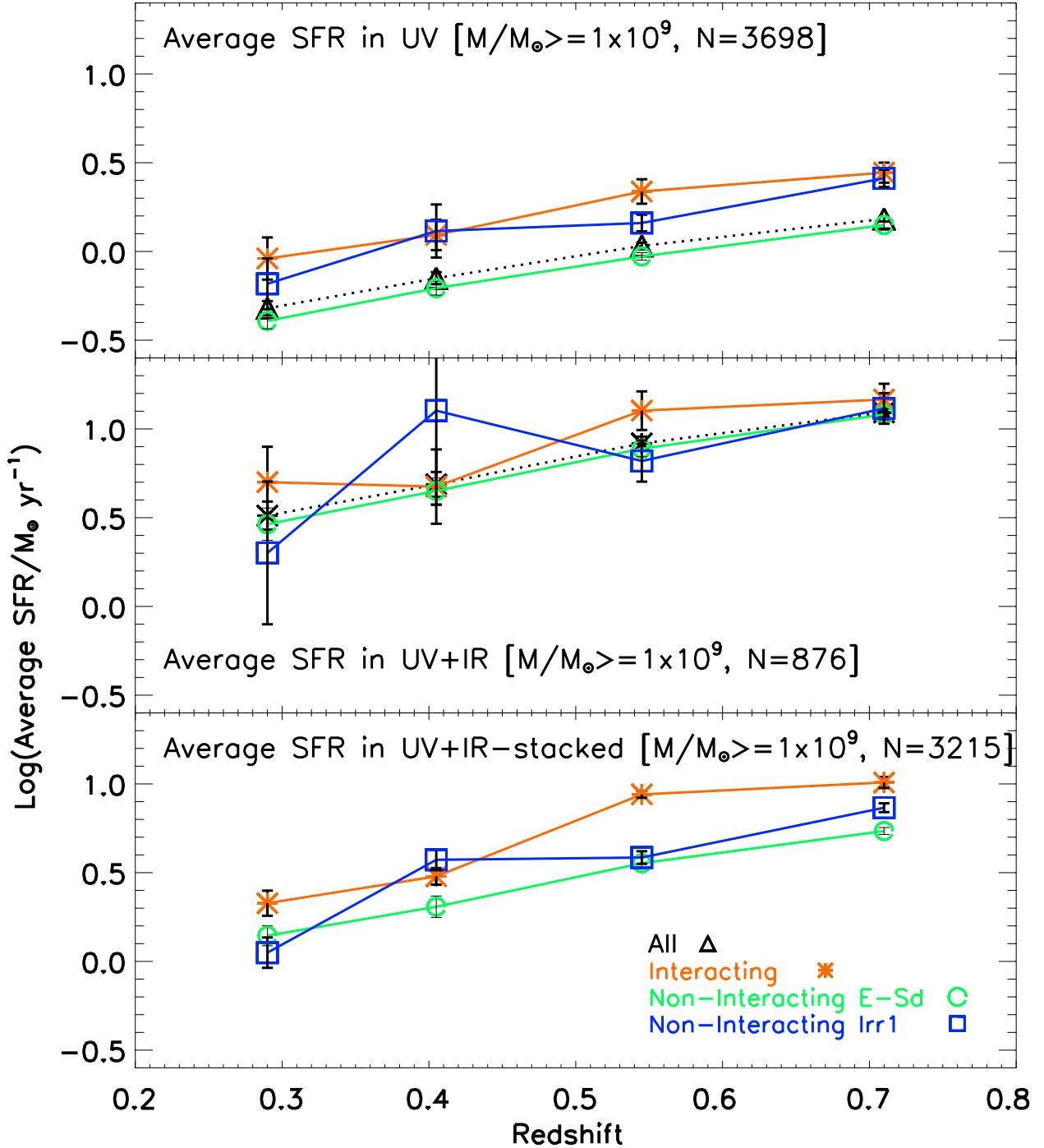
Fig. 13.— The average SFR of interacting, 'non-interacting E-Sd', and 'non-interacting Irr1' galaxies are compared over $z \sim 0.24$–0.80 for intermediate mass ($M \geq 1.0 \times 10^9 \ M_\odot$) galaxies. N denotes the number of galaxies used. The average UV-based SFR (top panel; based on 3698 galaxies), average UV+IR-based SFR (middle panel; based on only the 876 galaxies with 24um detections), and average UV+IR-stacked SFR (based on 3215 galaxies with 24um coverage) are shown. In all there cases, the average SFR of interacting galaxies is only modestly enhanced compared to non-interacting galaxies over $z \sim 0.24$–0.80 (lookback time ~ 3–7 Gyr).
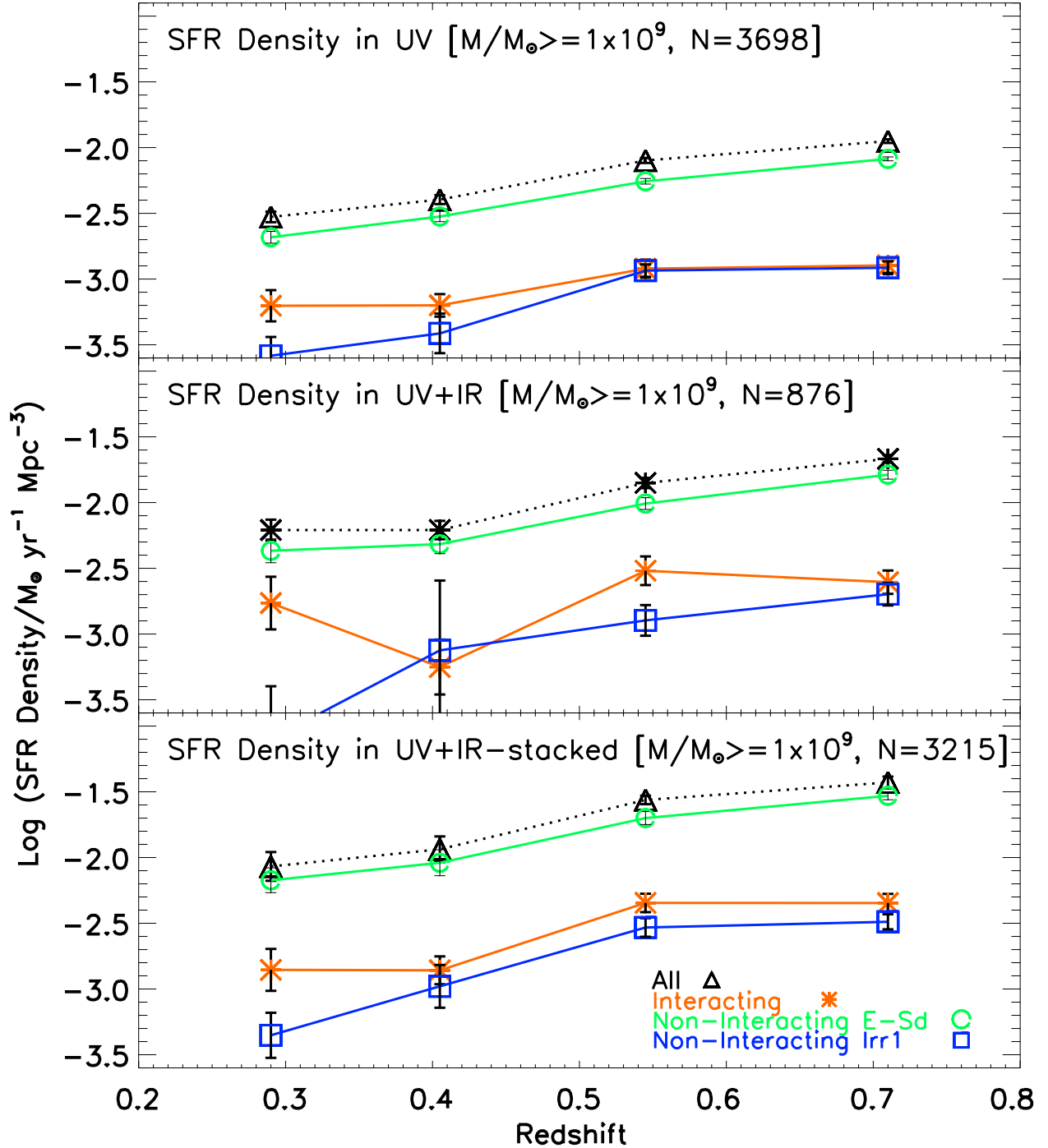
Fig. 14.— The SFR density of interacting, 'non-interacting E-Sd', and 'non-interacting Irr1' galaxies are compared over $z \sim 0.24$–0.80 for intermediate mass ($M \geq 1.0 \times 10^9 \, M_\odot$) galaxies. Results based on UV (top panel), UV+IR (middle panel), as well as UV+stacked-IR data (bottom panel), are shown in the top, middle, and bottom panels. In all bins, strongly interacting galaxies only contribute a small fraction (typically below 30%) of the total SFR density. In effect, the behavior of the cosmic SFR density over the last 7 Gyr is predominantly shaped by non-interacting E-Sd galaxies rather than strongly interacting galaxies.
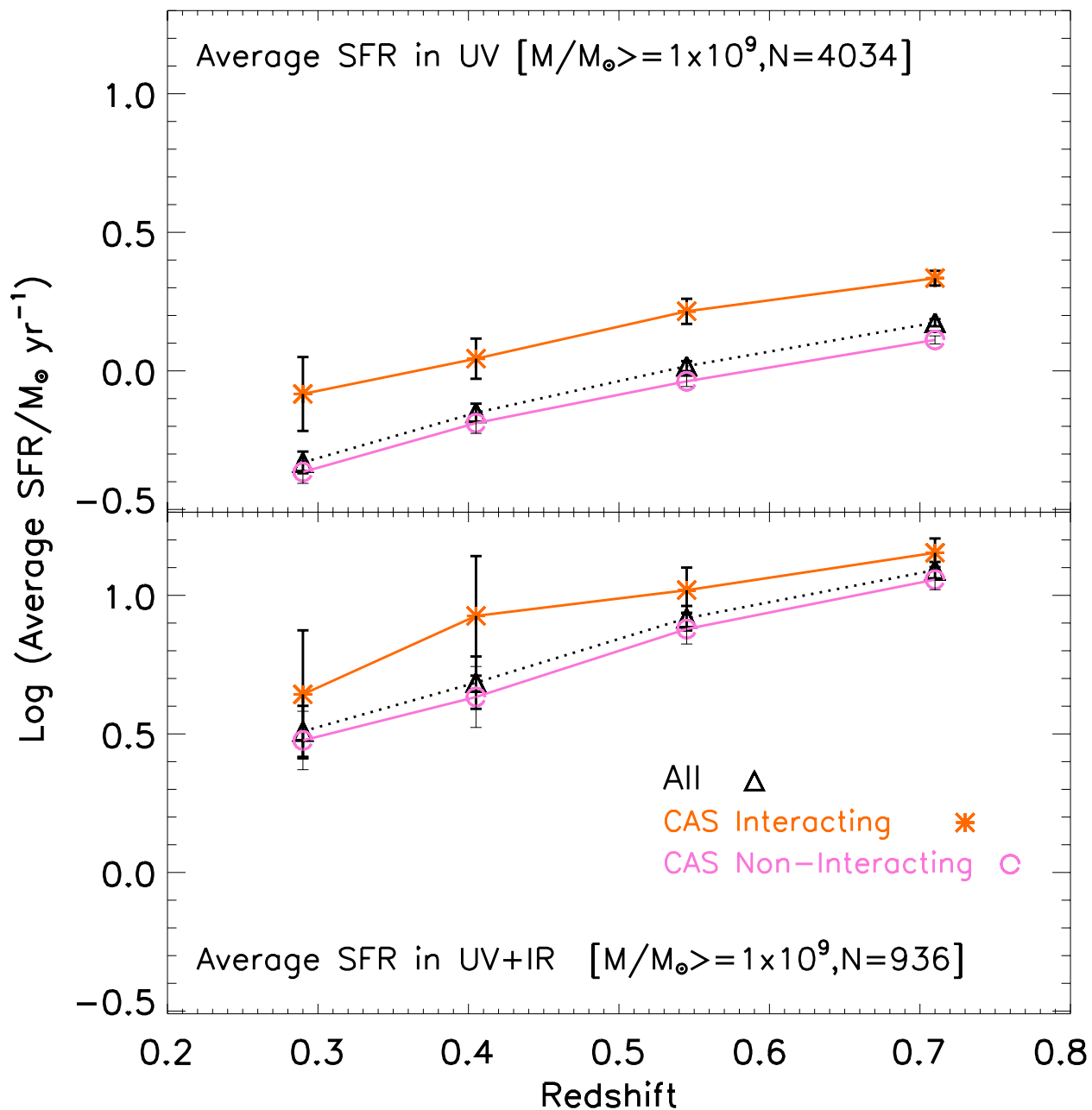
Fig. 15.— Same as in Fig. 13, but using the CAS merger criterion ($A > 0.35$ and $A > S$) to identify interacting galaxies. The average SFR of 'CAS-interacting' galaxies is only modestly enhanced compared to 'CAS non-interacting' galaxies, in agreement with the results from § 4.6.

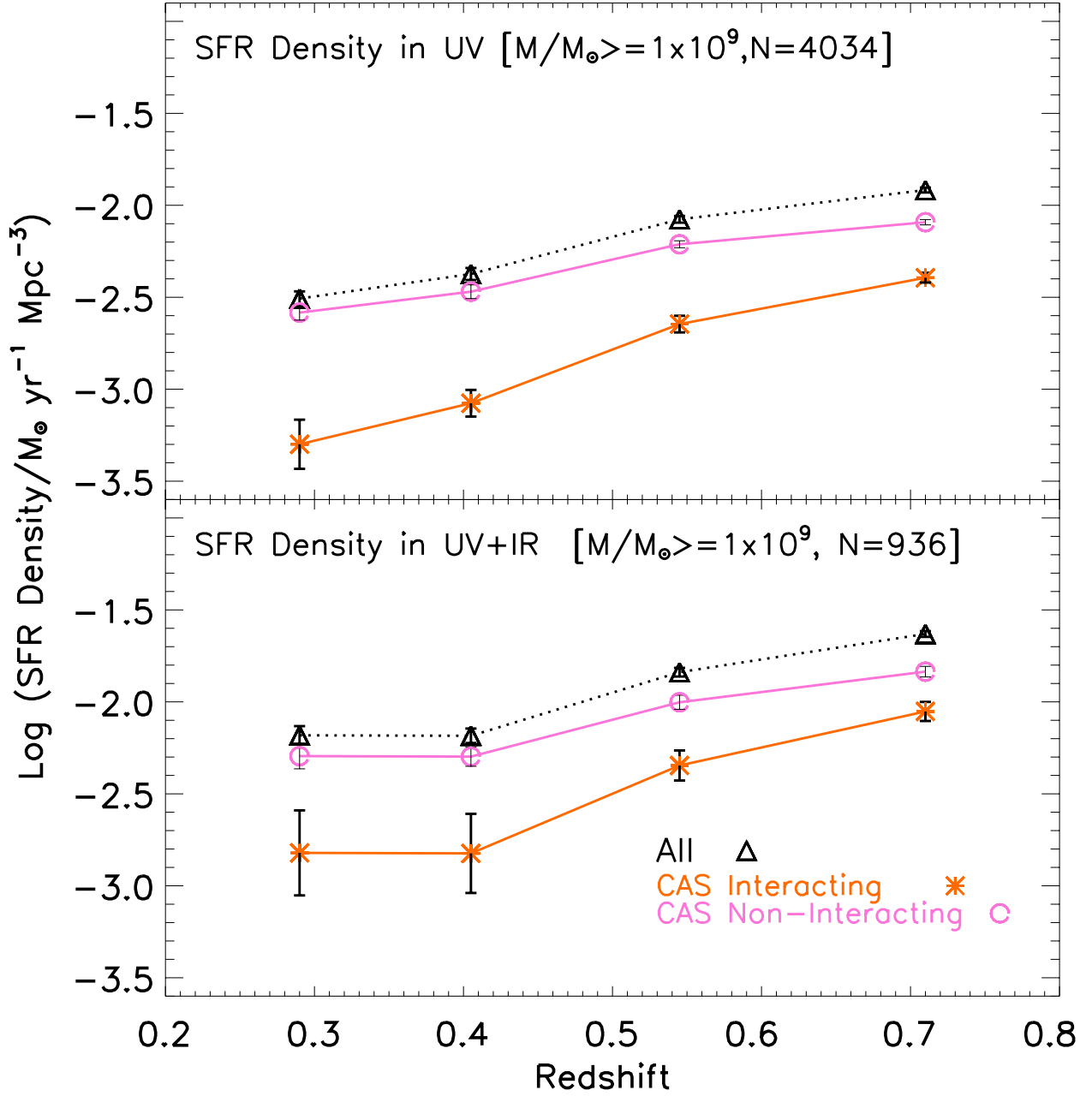Fig. 16.— Same as in Fig. 14, but using the CAS merger criterion ($A > 0.35$ and $A > S$) to identify interacting galaxies. 'CAS-interacting' galaxies contribute only 16% to 33% of the UV SFR density and 22% to 38% of the UV+IR SFR density. While the upper limits of these values are slightly higher than those based on the visual types (Fig. 14), the 'CAS non-interacting' galaxies' clearly dominate the SFR density.
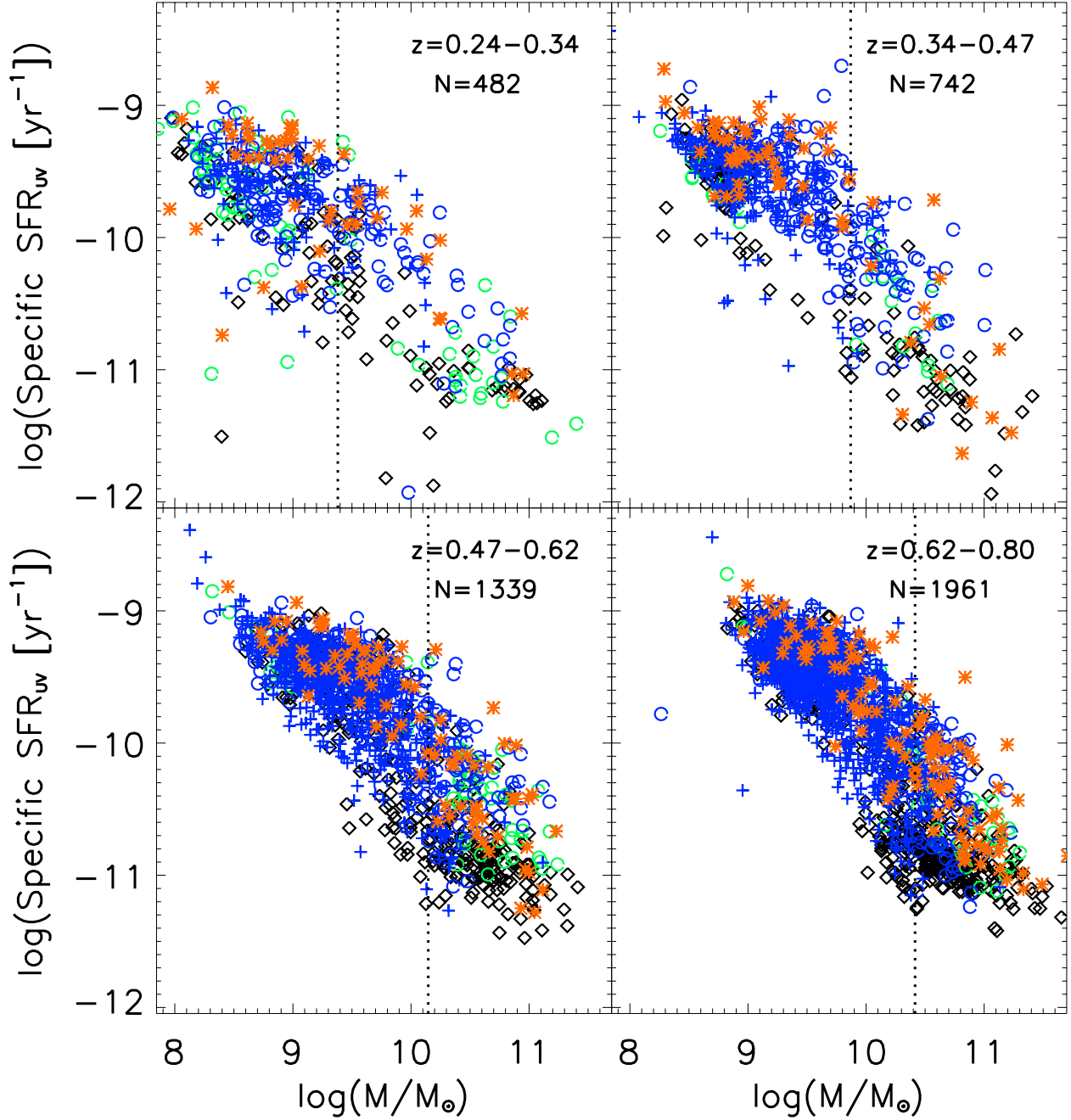
Fig. 17.— The specific SFR (defined as the SFR per unit stellar mass) based on UV data is plotted versus stellar mass. It ranges from 3×10^{-12} to 10^{-9} yr^{-1} and varies inversely with mass in all 4 redshift bins over $z \sim 0.24$–0.80. This is consistent with the idea that lower mass systems experience a larger fractional growth than high mass systems since $z < 1$, and that high mass systems have experienced the bulk of their stellar mass growth at earlier epochs ($z > 1$)

Table 1.   Visual Interaction Fraction for High Mass ($M \geq 2.5 \times 10^{10}\ M_\odot$) Sample S1 [N=789]

		1	2	3	4
(1)	Redshift bin	1	2	3	4
(2)	Redshift range	0.24–0.34	0.34–0.47	0.47-0.62	0.62–0.80
(3)	Lookback time [Gyr]	3.0–4.0	4.0–5.0	5.0–.6-0	6.0–7.0
(4)	$\lambda_{\rm rest}$ in F606W [Å]	4470–4414	4414–4023	4023–3651	3651–3286
(5)	Total no of galaxies	46	84	213	446
(6)	Fraction of Interacting	0.087±0.047	0.083±0.037	0.089±0.030	0.0807±0.025
(6a)	Lower limit on major merger fraction	0.022±0.021	0.035±0.022	0.014±0.009	0.011±0.006
(6b)	Lower limit on minor merger fraction	0.065±0.040	0.036±0.022	0.075±0.027	0.049±0.016
(6c)	Fraction of ambiguous minor/merger cases	0.00	0.012±0.012	0.00	0.020±0.008
(7)	Fraction of Non Interacting E-Sd	0.913± 0.241	0.869±0.229	0.878±0.229	0.785±0.205
(8)	Fraction of Non Interacting Irr1	0.000	0.024±0.018	0.009±0.007	0.025±0.010
(9)	Fraction of Compact	0.000	0.024±0.018	0.023±0.012	0.11±0.032

Note. — Rows are : (1) Redshift bin. (2) Range in redshift covered by the bin; (3) Range in lookback time covered by the bin; (4) Range in rest-frame wavelength traced by the F606W filter over the bin, assuming a pivot wavelength of 5915Å; (5) Total number of high mass galaxies per bin; (6) Fraction of galaxies visually classified as Interacting. These are likely candidates for interactions of mass ratio M1/M2> 1/10, including both major ($M1/M2 \geq 1/4$) and minor ($1/10< M1/M2 \leq 1/4$) mergers; (6a) Lower limit on the fraction of galaxies undergoing major interactions/mergers; (6b) Lower limit on the fraction of galaxies undergoing minor interactions/mergers; (6c) Remaining fraction of galaxies that could be either major or minor interactions/mergers; (7-9) Fraction of Non-Interacting E-Sd, Non-Interacting Irr1, and Compact.

Table 2.   Visual Interaction Fraction for $M \geq 1.0 \times 10^9\ M_\odot$ Sample S2 [N=3698]

(1)	Redshift bin	1	2	3	4
(2)	Redshift range	0.24–0.34	0.34–0.47	0.47-0.62	0.62–0.80
(3)	Lookback time [Gyr]	3.0–4.0	4.0–5.0	5.0–.6-0	6.0–7.0
(4)	$\lambda_{\rm rest}$ in F606W [Å]	4470–4414	4414–4023	4023–3651	3651–3286
	All [N=3698]				
(5)	Total no of galaxies	235	480	1117	1866
(6)	Fraction of Interacting	0.111±0.035	0.090±0.027	0.074±0.021	0.062±0.017
(6a)	Lower limit on major merger fraction	0.013±0.008	0.006±0.004	0.004±0.002	0.009±0.003
(6b)	Lower limit on minor merger fraction	0.038±0.016	0.021±0.008	0.021±0.007	0.017±0.005
(6c)	Fraction of ambiguous minor/merger cases	0.060±0.022	0.062±0.020	0.048±0.014	0.036±0.010
(7)	Fraction of Non Interacting E-Sd	0.850±0.220	0.846±0.220	0.796±0.207	0.793±0.206
(8)	Fraction of Non Interacting Irr1	0.064±0.023	0.052±0.017	0.108±0.030	0.064±0.018
(9)	Fraction of Compact	0.000	0.012±0.006	0.021±0.007	0.080±0.022
	Blue Cloud [N=2844]				
(10)	Total no of galaxies	154	332	876	1482
(11)	Fraction of Interacting	0.149±0.048	0.114±0.034	0.088±0.025	0.069±0.019
(11a)	Lower limit on major merger fraction	0.013±0.009	0.00	0.005±0.003	0.008±0.003
(11b)	Lower limit on minor merger fraction	0.046±0.020	0.024±0.010	0.023±0.008	0.016±0.005
(11c)	Fraction of ambiguous minor/merger cases	0.091±0.033	0.090±0.028	0.060±0.018	0.046±0.013
(12)	Fraction of Non Interacting E-Sd	0.753± 0.199	0.801±0.209	0.753±0.196	0.784±0.204
(13)	Fraction of Non Interacting Irr1	0.097±0.035	0.075±0.024	0.136±0.037	0.080±0.022
(14)	Fraction of Compact	0.000	0.009±0.006	0.023±0.008	0.067±0.018

Note. — Rows are : (1) to (9): As in Table 1, but for intermediate mass ($M \geq 1.0 \times 10^9\ M_\odot$) galaxies. However, note that the intermediate mass sample is incomplete for the red sequence. (10) to (14); Ditto, but for the blue cloud, where the sample is complete.

Table 3.   Interaction fraction in GEMS F606W (V) and GOODS F850LP (z) [N=855]

		GEMS V Average	GOODS z Average	GOODS z SJ	GOODS z SM	GOODS z KP
(1)	Fraction f of interacting galaxies	0.046±0.007	0.049±0.007	0.051±0.007	0.057±0.008	0.038±0.006
(2)	Ratio of f in GOODS z to GEMS V	-	1.06±0.22	1.10 ±0.23	1.20±0.25	0.83 ±0.18

Note. — As a test for bandpass shift and surface brightness dimming, the table shows a comparison of the fraction of interacting galaxies based on visual classification of GEMS F606W images and deeper redder GOODS F850LP galaxies. The sample consists of the 855 intermediate mass ($M \geq 1.0 \times 10^9$ $M_\odot$) galaxies at $z \sim$0.24 to 080, which are common to both GEMS F606W and GOODS F850LP surveys. Columns are: (2) Fraction f of interacting galaxies in GEMS F606W. The error bar only includes the binomial term $[f(1\text{-}f)/N]^{1/2}$; (3) Average Fraction f of Interacting galaxies in GOODS F850LP based on results by classifiers (SJ,SM,KP), shown in columns 4–6.